Design and Modeling of a Linear Array of Longitudinal Slots on Substrate Integrated Waveguide

Mahmud Tariq Rashid

A Thesis
in
The Department
of
Electrical and Computer Engineering

Presented in Partial Fulfillment of the Requirements
for the Degree of Master of Applied Science at
Concordia University
Montreal, Quebec, Canada
March 2006

Your file Votre référence
ISBN: 0-494-14278-2
Our file Notre référence
ISBN: 0-494-14278-2

Abstract

Design and Modeling of a Linear Array of Longitudinal Slots on Substrate Integrated Waveguide

Mahmud Tariq Rashid

In this thesis, the design of a broadside resonant linear array antenna of longitudinal slots on substrate integrated waveguide (SIW) for uniform aperture distribution and for a symmetric tapered distribution is presented. The concept of SIW has been proposed and used in which an "artificial" waveguide is synthesized and constructed with linear arrays of metallized via-holes or posts embedded in the same substrate used for the planar circuit. The SIW has been suitably converted to an equivalent rectangular waveguide. Elliott's modified design procedure including the internal higher order mode coupling, suitable for the usual range of thickness of the substrate, has been followed to obtain the optimum dimensions and positions of slots. The data for 'self-admittance' of an isolated slot as a function of its length and displacement, a requisite in Elliot's design procedure, has been generated by a commercially available full-wave finite element package Ansoft HFSS using an equivalent circuit for the slot with a subsequent extraction of Stegen-type curves. The validity and accuracy of the methodology have been compared with available published results for a slot on an X-band waveguide at 9.375 GHz.

The required aperture distribution which is the slot voltage distribution for a slot array antenna is obtained by fitting the array factor to Chebyshev's polynomial using Dolph-Chebyshev array synthesis procedure. The aperture distribution along with the polyfitted expressions of Stegen-type curves is then used in an iterative method to generate the design values of slots' lengths and offsets. The structure with dimensions found from this design is simulated and tuned to generate the radiation patterns and S-parameters. A transition between this waveguide and microstrip line is designed and optimized and the impedance bandwidth is studied. The methodology has been utilized to design two linear arrays. Numerical results are presented and discussed for several cases.

Acknowledgement

First of all I would like to express my deepest gratitude to my thesis supervisor, Dr. A. Sebak, for his continuous guidance and support throughout my thesis work. His vast experience, immense knowledge and great personality are always the source of great inspiration, which have made the completion of this thesis possible.

I want to acknowledge those people who helped me during my thesis work. Dominic Deslandes of University of Montreal and Sadegh Farzaneh of Concordia University have provided some valuable practical advice.

I would like to express my appreciation to my parents, brothers for their continuous support and encouragement.

Table of Contents

List of Figures

List of Tables

List of Abbreviations

ABC	Absorbing Boundary Condition
BI-RME	Boundary Integral Resonant Mode Expansion
CPW	Coplanar Waveguide
dB	Decibel
FDTD	Finite Difference Time Domain
FETD	Finite Element Time Domain
GEO	Geostationary Earth Orbit
HFSS	High Frequency Structure Simulator
IC	Integrated Circuits
LMDS	Local Multipoint Distributed Systems
LTCC	Low-Temperature Co-Fired Ceramics
MIC	Monolithic Integrated Circuit
MMIC	Monolithic Microwave Integrated Circuit
PCB	Printed Circuit Board
PEC	Perfect Electric Conductor
PML	Perfect Matching Layer
Q-factor	Quality Factor
RF	Radio Frequency
SIC	Substrate Integrated Circuit
SIRW	Substrate Integrated Rectangular Waveguide

SIW	Substrate Integrated Waveguide
SLL	Side Lobe Level
TE	Transverse Electric
TEM	Transverse ElectroMagnetic
TM	Transverse Magnetic
VSWR	Voltage Standing Wave Ratio

List of Symbols

Symbol	Meaning
k	Wave number
$c0$	Velocity of light
η	Impedance of free space
β_{10}	Propagation constant of the TE_{10} mode
β_{SIW}	Propagation constant of the SIW
ε	Permittivity of the dielectric filling the waveguide
ε_{eff}	Effective dielectric constant of the substrate
μ_0	Permeability of free space
γ_{mn}	Propagation constant of the *mn* th mode
λ	Wavelength
λ_g	Guide wavelength
x_0	Offset of slot from the side wall of the waveguide
x	Offset of slot from the centerline of the broadwall of the waveguide
l	Half –length of slot
w	Width of slot
a_{RWG}	Width of broad wall of the equivalent rectangular waveguide
l_r	Resonant length of a slot

G_r	Resonant conductance of a slot
$\vec{E}$	Electric field intensity
$\vec{K}$	Linear electric current density
$\vec{H}$	Magnetic field intensity
V_n^s	Slot voltage of nth slot
A_{10}^n	Complex amplitude of incident wave of TE_{10} mode on nth slot from $z<-l_n$
D_{10}^n	Complex amplitude of incident wave of TE_{10} mode on nth slot from $z>l_n$
Y_n^a	The active admittance of the n th slot (including mutual coupling)
V_n	Mode voltage on the equivalent transmission line at the site of Y_n^a;
B_n	Back scattered wave from Y_n^a
C_n	Forward scattered wave from Y_n^a
Y	Self Admittance of a slot
G_0	Characteristic conductance of the waveguide
B_{10}	Complex amplitude of the back scattered TE_{10} mode.
C_{10}	Complex amplitude of the forward scattered TE_{10} mode.
θ	Elevation angle
ϕ	Azimuth angle

Chapter 1

Introduction

1.1 Introduction

Waveguide slot array antennas are an important class of microwave antennas with numerous applications such as radar and communication systems. Rectangular waveguides play an important role in realizing the high performance RF passive components due to their high Q-factor and high power capacity. However, the conventional waveguides have the disadvantage of large sizes and require complex transitions for integration with planar circuits. Typical integration schemes from rectangular waveguide with planar structure are bulky and usually require a precision machining process, which is difficult to achieve at millimeter-wave frequencies for mass production. Multi-layered printed circuit boards (PCB) and low-temperature co-fired ceramics (LTCC) circuits are the two low-cost RF fundamental building blocks. It is important to look into alternatives with multilayered LTCC or PCB. Recently, some works have been reported to discuss such structures, called substrate integrated waveguides (SIW) which are useful for the design of millimeter-wave circuits such as filters, resonators etc. Also, an SIW can easily be connected to microstrip or coplanar circuits using simple transitions. The SIW together with other types of synthesized waveguide can be generalized by a new concept called "substrate integrated circuits (SICs)" that allows the integration of planar and nonplanar structures within the same substrate.

1.2 Objective and Motivation :

In this thesis, we present the design of a broadside resonant linear array antenna of longitudinal slots at 30 GHz (Ka-band) on substrate integrated waveguide with Rogers RT /Duroid 5880 substrate (ε_r =2.2, loss tangent = 0.0009). The designed antenna could be a choice for the antenna used in Ka-band LMDS (local multipoint distributed systems). Waveguide slot array antenna is a proposed solution for upcoming new Ka-band satellite communication systems, based on a constellation of Geostationary Earth Orbit (GEO) satellites; the mobile satellite terminal transmitting at 30 GHz being a key part of the system. By transferring the conventional waveguide slot array antenna to the substrate integrated waveguide (SIW) structure, the advantages of the slot array antenna as well as the advantages of the SIW such as small size, low profile, low cost can be obtained.

In this thesis, design of a broadside resonant linear array antenna of longitudinal slots on SIW, for uniform aperture distribution(~ -13.5 dB side-lobe level) and a lower side-lobe level (-20 dB) have been discussed. A modified Elliott's procedure [1] and [2] including the internal high order mode coupling, which is suitable for the usual range of thickness of the substrate, has been followed. A commercial finite element software, Ansoft HFSS [3], has been used to generate radiation pattern and S-parameter results. The finite element method (FEM) is a numerical technique that has been employed in diverse areas such as waveguide problems, electric machines, semiconductor devices, microstrips etc. [4]. The method works by discretizing the solution region into finite number of subregions or elements, deriving governing equations for a typical element, assembling of all elements in the solution region and

finally solving the system of equations obtained. The accuracy of the solution depends on the size of each of the individual elements.

Though in recent years several microwave sources and circuits have been studied, very little have been studied and published so far on the optimum antenna structure for use with substrate integrated waveguides. In this thesis, we present the development and the design procedure for linear array antenna on SIW for uniform distribution and symmetric tapered distribution.

1.3 Overview of this thesis

The chapters of this thesis have been presented in following way.

Chapter 2 discusses the review of literature of related work. It discusses early classical work on impedance properties of a slot on the broad wall of an air-filled rectangular waveguide and subsequent design procedures of slot arrays on a waveguide. Later it discusses the evolution of substrate integrated waveguide (SIW), a reliable candidate for low-cost mass production of millimeter-wave circuits and systems and the transformation of design procedure of slot array for SIW.

Chapter 3 discusses the theory of slot array on SIW. The conversion technique of an SIW to an equivalent rectangular waveguide is addressed first. Three design equations necessary for slotted array antenna on the broad wall of a dielectric-filled waveguide have been developed and discussed starting with the *E*-field distribution induced in the slot. It can be known by modeling the actual situation with a 'zero' wall thickness and applying boundary condition for tangential magnetic field, *H* at all points in the slot aperture. In the process of theory development, concept of self-admittance, active admittance, slot voltage, mode voltage and their relation and analytical formulation of

mutual coupling have been presented and input matching has been taken into consideration.

Chapter 4 presents results of a single slot on broadwall of SIW. The impedance properties of an isolated slot are presented. The crucial thing for a slotted array antenna design using Elliot's design procedure is to know the normalized self-admittance, $\frac{Y}{G_0}$ of an isolated slot for the useful range of lengths and offsets, where Y is the slot admittance and G_0 is the characteristic conductance of the equivalent rectangular waveguide. This information can be obtained by measurement, by using computational technique like FDTD, by scaling a known measurement data, or by using simulation software for shunt model of a longitudinal slot. If the slot is represented by shunt admittance in an equivalent transmission line which is true in case of symmetrical scattering, $\frac{Y}{G_0}$ can be calculated from scattering parameters using equivalent circuit for a longitudinal slot.

With this idea, the commercially used finite element software Ansoft HFSS [3] has been carefully explored to generate $\frac{Y}{G_0}$ as a function of lengths and offsets. The validity of this methodology has been verified with available published results for a slot on an *X*-band waveguide at 9.375 GHz. From the data of $\frac{Y}{G_0}$ thus generated, Stegen-type of curves -conductance and susceptance both normalized by resonance conductance and resonant length versus offset and resonance conductance versus offset curves were derived. These curves have been suitably polyfitted into expressions to be later used in array design.

Chapter 5 presents the results of designed arrays with four longitudinal slots. For a resonantly spaced broadside array (array elements half-guide-length apart), the progressive phase shift between elements is zero. The required aperture distribution which is the slot voltage distribution for a slotted array antenna is obtained by fitting the array factor to Chebyshev's polynomial. The aperture distribution along with the polyfitted expressions of Stegen-type curves from Chapter 4 are then used in an iterative method to generate the design values of lengths and offsets as discussed in Chapter 3. The structure with lengths and offsets thus obtained is simulated and tuned to generate the desired radiation patterns and best possible input match. Finally a transition between this waveguide and microstrip line is designed and optimized and the impedance bandwidth is studied. The design methodology is extended for eight slots and results of simulation are presented.

In Chapter 6, conclusive comments have been made. The methodology, its advantage and limitations have been discussed critically. The extension of the current work, in this recent area of mm wave SIW, is forecasted.

Chapter 2

Literature Review

2.1 Introduction

This chapter discusses the review of literature of previous related work. It starts with early classical work of Steveson, Oliner, Stegen ([5]-[7]) that formulated impedance properties of a slot on broad wall of an air-filled rectangular waveguide and then discusses design procedures for slot arrays on waveguides by Elliott, Yee and others ([11]-[13]). The literature on properties of substrate integrated waveguide (SIW) and circuits and systems with SIW have been overviewed. Finally the research works on evolution of design of slot array for an SIW from a dielectric-filled rectangular waveguide are presented.

2.2 Impedance properties of a slot on broad wall of an air-filled rectangular waveguide

Stevenson is regarded as the pioneer of research work related to a slot on a rectangular waveguide. Stevenson [5] published a classic paper in which he established the internal Green's functions for a rectangular waveguide and used those functions to analyze scattering off a longitudinal slot excited by an incident TE_{10} mode. With the assumptions of resonant length slot, transverse electric field that possessed an equiphase and half-cosinusoid amplitude distribution, Stevenson was able to show that dominant TE_{10} mode scattering off the slot was symmetrical, as a

result of which the slot could be represented by a shunt element on an equivalent transmission line.

Stegen [6] carefully performed a series of experiments to measure relative backscattering from longitudinal slots cut in a broad wall of standard *X* band waveguide (*a* = 0.900 inch, *b* = 0.400 inch, *t* = 0.050 inch) at a frequency of 9.375 GHz. Stegen wanted to achieve a standard against which theory could be judged, and it is a tribute to his painstaking work that his data is still serving as the standard. Stegen found that resonant length, contrary to Stevenson's assumption, was offset-dependent.

Oliner [7] developed the first theory for longitudinal slots which would permit calculation of the susceptance as well as the conductance both at and away from resonance by the use of variational expressions coupled with certain stored power considerations. Oliner was able to derive a wall thickness correction by treating the thickness of the slot as a section of stub waveguide. He also developed a correction factor for square-ended slots.

The next significant work on this problem was undertaken by Khac *et al.* [8]. They used Stevenson's internal Green's function and the external half-space Green's function to formulate integral expressions (involving the unknown slot aperture electric field) for the internal and external scattered fields, and matched the total longitudinal *H*-field across the slot aperture. Khac then used the Method of Moments, employing pulse functions and point matching, to solve for unknown slot aperture electric field and used that knowledge to find the dominant mode backscattering, and thus normalized slot admittance.

Chao Liu *et al.* [9] used the Finite Difference Time Domain (FDTD) method for solving the electric field in the longitudinal resonant slot of waveguide and the far

field radiation pattern. The FDTD method is a full-wave analysis algorithm, through numerical calculations, the radiating or scattering characteristics can be obtained through Fourier transformation within the whole bandwidth.

Brown [10] has pointed out that if computer resources permit, the necessary data to design a waveguide slotted array can be gathered with minimal input from the user through the use of commercially available finite element software. The scattering matrices of the radiating slots can be completely characterized using the finite element software and the self admittance of the radiating slot is obtained from the scattering matrix data which is a function of frequency, slot-offset and slot length if a rectangular type of slot is used. Elliot's design procedure [1] can then be used to design the appropriate slot offsets and lengths.

2.3 Design of array antenna of longitudinal slots on broad wall of a rectangular waveguide

A significant design procedure of slotted-array antenna on the broad wall of an air-filled waveguide was described by Elliott and Kurtz [11]. The design equation arose from linking the performance of the slot array to that of an equivalent dipole array via Babinet's principle. One needs to place the load impedance in series with the equivalent dipole to account for the fact that the resonant length of the slot is affected by its offset. A general relation between the slot and mode voltages was developed, and then formulas were derived for the active, self, and mutual admittances among slots. These formulas resulted in a design procedure.

If the waveguide is filled with a material whose dielectric constant differs sensibly from unity, the design approach [11] of equivalent array of loaded dipoles for slotted-array is no longer valid. Elliott [1] improved the design procedure with a more realistic approach. Through the use of reciprocity theorem, he developed the causes

of slot voltage V_s which are TE_{10} modes passing underneath the slot in both directions plus external coupling to the other slots in the array and also developed the expression for mutual coupling.

Elliott and Loughlin [2] found that in a waveguide of reduced height, the slot's resonant length increases. This means that the tip-to-tip distance between successive slots in the same waveguide is less, indicating that the higher order modes scattered off one slot are less attenuated when they reach a neighboring slot. An analytical solution showed justification to assume that internal higher order mode coupling would consist solely of TE_{20} contributions. They modified design procedure of [1] to include contribution of TE_{20} in slot voltage and mutual coupling.

Sangster *et al.* [12] emphasized theoretically evaluated self-admittances to overcome the increasingly unnecessary restriction of relying on measured self-admittances and developed a computer aided design/synthesis procedure for slot array antennas on waveguide. The synthesis was based to a large extent on the method described by Elliott and Kurtz [11], but it incorporated a number of essential modifications to accommodate the inclusion of the Method of Moments, which was introduced to compute the self-admittances of individual apertures.

The required computer cost and the excessive computer time restrict the design procedure in [11] and [12] to small slot arrays (less than a few tens of slots).Yee [13] focused on the design of large arrays. He adopted infinite array model outlined in [6] and assumed radiated power to be proportional to slot active conductance and equated the phase to the active admittance phase. A Method of Moments type solution using the uniformly excited infinite array model yielded the approximate values of the slot active admittances in the array environment.

Bastani *et al.* [14] used the Method of Moments to analyze large planar slotted-waveguide arrays to overcome the limitations of assumption of zero wall thickness or a stub waveguide for slot of [13].

2.4 Via holes

Before proceeding to discuss substrate integrated waveguide and several associated circuits, via holes, being part of SIW, should be addressed first. The miniaturization and large scale integration of electronic devices place an increasing demand on multilayer interconnect geometries. Via holes are one of the most common discontinuities in multilayer circuits.

Antonini *et al.* [15] used the Finite Difference Time Domain (FDTD) method to extract the equivalent circuit for the via in a multilayer printed circuit boards from scattering parameters. Dongsoo *et al.* [16] used hybrid full-wave analysis using FDTD and finite-element time-domain (FETD) methods to calculate the scattering parameters of single and multiple cylindrical via holes in a microstrip structure. In microstrip technology, short-circuits are commonly produced, for both MIC and MMIC applications, by means of vias through the dielectric.

Laso *et al.* [17] have shown through theoretical analysis and experimental results that via holes act as broadband reflectors or short-circuits with enhanced behavior at high frequencies. They have analyzed a single via hole and via holes with one half-wavelength separation periodically arranged along a microstrip line. The reflectivity increases significantly as number of vias go up.

Uchimura *et al.* [18] built a waveguide of new structure for millimeter-wave applications. The dielectric waveguide with glass-ceramic substrate was constructed with sidewalls consisting of lined via-holes and edges of metallized planes. This

structure can be manufactured by lamination techniques, with same process that of ceramic circuit boards and packages. Insertion loss per unit length of the guide was estimated to be less than 0.5 dB/cm at 83 GHz. Electromagnetic simulation, confirmed the realization of that fundamental structures, such as bends, branches, power dividers with sufficient performances.

Ali Zeid *et al.* [19] have studied the problems of electromagnetic isolation between elements of microelectronic circuits. Metallic rods disposed periodically in cascade have been treated. They used multimodal variational method for both TE and TM polarized incident electric field to calculate the impedance of cascaded screens and the reflection coefficient. From the study of dispersion curves they illustrated the waveguide design between two grids of periodically arranged metallic holes.

2.5 Substrate integrated waveguide (SIW)

Substrate integrated waveguide is made of a periodic via-hole structure to realize bilateral edge walls. Figure 2.1 shows a substrate integrated waveguide with periodic metallic via holes. A substrate integrated waveguide can largely preserve the advantages of conventional rectangular waveguides such as high Q factor and high

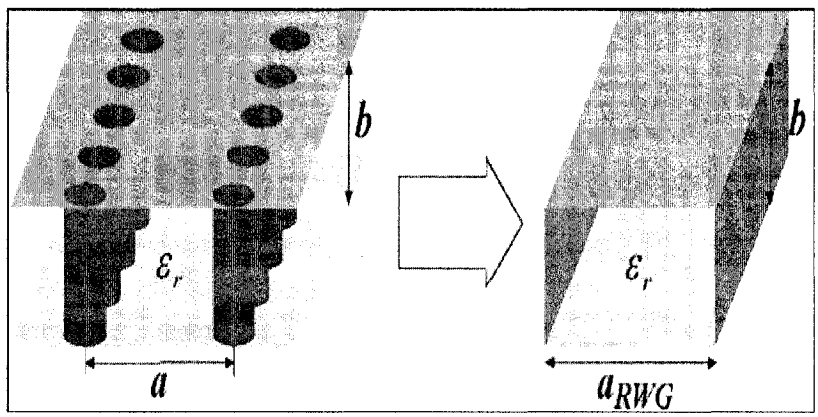

Figure 2.1: Configuration of SIW synthesized using metallic via-hole arrays and the equivalent rectangular waveguide [29].

power capacity. In Figure 2.1, b is the substrate height and a is the distance between parallel array of via holes. As shown in Figure 2.1, the substrate integrated waveguide having a dielectric constant ε_r is equivalent to a dielectric-filled rectangular waveguide having width a_{RWG} and dielectric constant ε_r.

Cassivi *et al.* [20] have shown that the substrate integrated rectangular waveguide (SIW) basically has the same guided-wave characteristics as the conventional rectangular waveguide. Using the 'Boundary Integral Resonant Mode Expansion' (BI-RME) method combined with the Floquet's theorem they obtained the dispersion properties of the SIW and derived empirical equations to estimate the cutoff frequency of the first two dominant modes of the SIW and the effective width for the dominant mode.

Deslandes and Wu [21] have presented three simple design steps to transform a substrate integrated waveguide to an equivalent rectangular waveguide using a commercial finite-element software package HFSS and discussed the design of *H*-plane step, post resonator, 90^0 bend and 90^0 curvature using posts on a substrate integrated waveguide.

Zhang et al. [22] have developed a novel finite difference frequency domain (FDFD) algorithm for the analysis of guided-wave problems of substrate integrated waveguide where the Floquet Theorem has been employed and Perfect Matching Layer (PML) has been chosen as Absorbing Boundary Condition (ABC).

The integrated planar technique has been considered as a reliable candidate for low-cost mass production of millimeter-wave circuits and systems. Integrating planar and non-planar circuits on a substrate can significantly reduce size, weight, and cost, and greatly enhance manufacturing repeatability and reliability.

Deslandes and Wu [23] have presented new concepts that allow for a complete integration of planar circuits and waveguide filters synthesized on a single substrate by means of metallized post (or via-hole) arrays. Design criteria were presented for the post pitch and diameter for an inductive post type filter. An experimental three-pole Chebyshev filter having 1-dB insertion loss and return loss better than 17 dB was demonstrated.

Cassivi and Wu [24] have designed a low-cost microwave oscillator working at 12.02-GHz using substrate integrated waveguide (SIW) cavity that acts as a frequency selector as well as a feedback-coupling device. Che *et al.* [25] developed the analytical model of the ferrite phase shifter in SIW and introduced necessary formulae.

2.6 Design of array antenna of longitudinal slots on a substrate integrated waveguide (SIW)

Design and simulation of circuits on SIW necessitates first to find an equivalent dielectric-filled waveguide of SIW. One of the methods of [20] or [21] can be followed for that. The next step is to obtain the self-admittance of an isolated longitudinal slot on SIW. Gatti *et al.* [26] discussed an FDTD method for computation of the equivalent circuit of an isolated longitudinal slot cut in the broad wall of a dielectric-filled rectangular waveguide. High numerical efficiency has been obtained by using Stegen's factorization [6] of the slot admittance.

Very recently some works of slotted antennas on SIW have been published [27], [28], [29] where [27] has dealt with dual slot resonant antenna and [28] has discussed about a single slot antenna at *W*-band using photoimageable thick film technology.

Yan *et al.* [29] proposed an integrated four-by-four slot-array antenna at *X*-band by etching longitudinal slots on the top metallic surface of the substrate integrated waveguide which was fed by a microstrip power divider. A new experimental formula was given for the normalized width of the equivalent waveguide. The SIW slot array was designed for a uniform aperture distribution using a modified Elliott's procedure [2].

2.7 Transition between planar circuit and rectangular waveguide

A rectangular waveguide can be used to design high Q components but requires complex transitions to integrated planar circuits. Several studies of transitions between microstrip line and rectangular waveguide have been reported [30]–[32].

Typical integration schemes from rectangular waveguide with planar structure are bulky and usually require a precision machining process, which is difficult to achieve at millimeter-wave frequencies for mass production.

A straightforward solution is to integrate the rectangular waveguide into the microstrip substrate. This will reduce the Q factor of the waveguide because of dielectric filling and volume reduction, but the entire circuit including planar circuit, transition and waveguide can be constructed using standard PCB or other planar processing techniques.

Deslandes *et al.* [33] developed a new planar platform instead of a three-dimensional (3-D) complex mounting structure in which the microstrip line and rectangular waveguide are fully integrated on the same substrate. The transition structure makes use of a tapered microstrip line to excite the waveguide mode of the SIW.

Experiments at 28 GHz showed that an effective bandwidth of 12% at 20 dB return loss was obtained with an in-band insertion loss better than 0.3 dB.

In [34], a new planar platform was developed in which a coplanar waveguide (CPW) and a rectangular waveguide are fully integrated on the same substrate and they are interconnected via a simple transition. They can be built with a standard PCB process. Experiments at 28 GHz show that an effective bandwidth of 7% at 15 dB return loss can easily be achieved.

Chapter 3

Design of slotted waveguide array antenna

3.1 Introduction

In a microwave system, active devices in the form of chips are often surface-mounted on a planar carrier substrate, while the high-Q passive components like diplexers and filters are usually designed on the basis of rectangular waveguides or other non-planar structures. Because of the high cost and large size of rectangular waveguide components, the concept of substrate integrated rectangular waveguide (SIW) has recently been studied and developed. A substrate integrated waveguide is made of a periodic via-hole structure to realize bilateral edge walls. Such SIW structures can largely preserve the advantages of conventional rectangular waveguides such as high Q factor and high power capacity. The idea of synthesizing rectangular waveguide in planar form on a single substrate leads to the design and development of low-cost millimeter-wave integrated circuits (ICs) and systems. In this way, a system can be integrated even in a package, reducing size, weight, and cost, and greatly enhancing manufacturing repeatability and reliability.

In this chapter, design equations necessary for a slotted array antenna on the broad wall of an SIW have been developed and discussed starting with an E-field distribution induced in the slot. The design procedure of a slotted array antenna on a substrate integrated waveguide starts with conversion of the SIW to an equivalent

rectangular waveguide. Once the dimension (the width) of the equivalent rectangular waveguide is found, the next thing is to follow the design procedure of slotted array antenna for a dielectric-filled waveguide with width found earlier. All the existing design procedures and theory developed for the rectangular waveguide are directly applicable to its synthesized counterpart [23]. In the process of theory development, the concepts of self-admittance, active admittance, slot voltage, mode voltage and their relation and analytical formulation of mutual coupling have been presented and input matching has been taken into consideration.

3.2 Equivalent rectangular waveguide using an SIW

A substrate integrated waveguide is made of a periodic via-hole structure to realize bilateral edge walls.

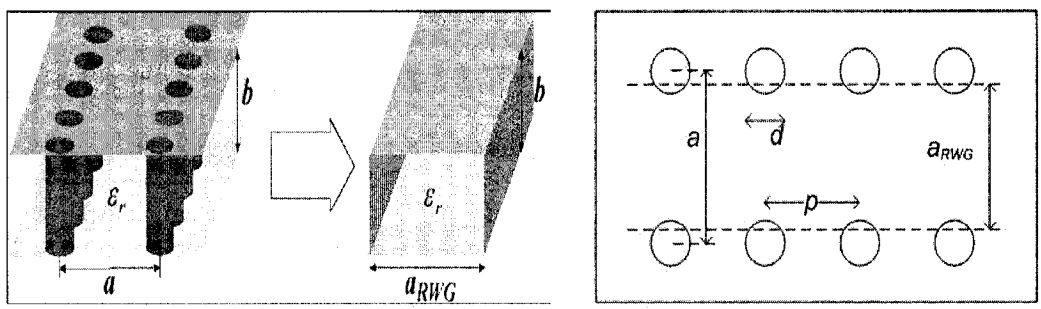

(a) (b)

Figure 3.1: (a) SIW and the equivalent rectangular waveguide [29]

(b) Top view of an SIW.

Figure 3.1 (a) shows a substrate integrated waveguide with periodic metallic via holes and Figure 3.1 (b) shows its top view. In Figure 3.1(a) and (b), b is the substrate height, a is the distance between parallel array of via holes, p is the period or distance between successive via holes and d is the via hole diameter.

It is necessary to convert the SIW to an equivalent rectangular waveguide that has the same propagation constant and characteristic impedance as those of the SIW to follow the design procedure of a slot array antenna on broadwall of a dielectric-filled waveguide.

It is established that periodic via holes in a SIW act as short circuit or perfect electric conductor (PEC) sidewalls ([17]-[19]) and an SIW with via holes has the same guided-wave characteristics as the conventional rectangular waveguide [20]. In [20] dispersion properties of the substrate integrated waveguide have been obtained by applying Floquet's theorem and 'Boundary Integral Resonant Mode Expansion' (BI-RME) method, and useful empirical equations have been derived to estimate the first two cut-off frequencies of the first two dominant modes i.e. TE_{10}-like and TE_{20}–like modes. The equations of cut-off frequencies are

$$f_c(TE_{10}) = \frac{c0}{2\sqrt{\varepsilon_r}}\left(a - \frac{d^2}{0.95 \times p}\right) \tag{3.1}$$

and

$$f_c(TE_{20}) = \frac{c0}{\sqrt{\varepsilon_r}}\left(a - \frac{d^2}{1.1 \times p} - \frac{d^3}{6.6 \times p^2}\right) \tag{3.2}$$

and thus from Figure 3.1, a_{RWG}, the width of broad wall of the equivalent rectangular waveguide, is related to center to center distance (a) between parallel sets of via holes, via hole diameter d, and inter via spacing or pitch p of adjacent via holes in the linear array by this equation.

$$a_{RWG} = a - \frac{d^2}{0.95 \times p} \tag{3.3}$$

The accuracy of equation (3.1) is within $\pm 5\%$ and for equation (3.2), a precision better than $+4\%/-9\%$ is possible [20]. The approximations are valid for $p<\lambda_0\sqrt{\varepsilon_r}/2$, and $p<4d$ where λ_0 is the free-space wave length and ε_r is dielectric constant of the substrate.

Equation (3.3) can be used to design an equivalent rectangular waveguide of an SIW. However, a more accurate and frequently used technique [21], [23] has been used to calculate the propagation constant and hence to get a_{RWG}.

In this method, two straight SIW sections of different lengths L_1 and L_2 ($L_1 > L_2$) are simulated. For simplicity the difference is chosen to be less than one guide wavelength.

The difference in phase of transmission coefficients for TE_{10} mode at L_1 and L_2 are $e^{-j\beta_{SIW}\times L1}$ and $e^{-j\beta_{SIW}\times L2}$, respectively, where β_{SIW} is the propagation constant of the SIW. Since $\angle S^{L2}{}_{21}$ and $\angle S^{L1}{}_{21}$ can be computed from simulations, β_{SIW} can be calculated straightforward by

$$\beta_{SIW} = \frac{\angle S^{L2}{}_{21} - \angle S^{L1}{}_{21}}{L_1 - L_2} \tag{3.4}$$

And $$a_{RWG} = \frac{\pi}{\sqrt{(\omega^2\mu_0\varepsilon_0\varepsilon_r - \beta^2_{SIW})}} \tag{3.5}$$

3.3 Principle of radiation from a slot on a waveguide

When a guiding structure is composed of a good conductor, which is usually the case, the linear electric current density $\vec{K}$ on the conductor surface can be found from

$\vec{K}=\hat{n}\times\vec{H}$, where $\hat{n}$ is a unit vector normal to the conductor surface and $\vec{H}$ is the magnetic field for the particular mode, evaluated at the surface of the conductor. If a narrow slot is cut in the conductor surface and is open to outer space, then radiation can occur through the interruption of $\vec{K}$. A family of such slots constitutes an antenna array.

Most application of the array antenna with abovementioned idea involve the use of rectangular waveguide as the guiding structure, with transverse dimension chosen so that only the TE_{10} mode can propagate. Figure 3.2 shows the instantaneous distribution of current on the upper broad wall. Over time, this pattern will propagate longitudinally at the phase velocity of the TE_{10} mode.

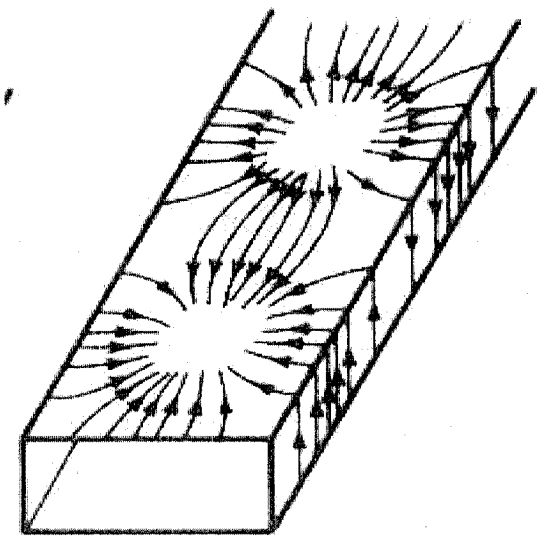

Figure 3.2: The instantaneous distribution of current on the upper broad wall for TE_{10} mode [35].

The most commonly used slots are shown in Figure 3.3. A longitudinal slot cut into the wall of a waveguide interrupts the transverse current flowing in the wall, forcing the current to travel around the slot, which induces an electric field in the slot. The position of the slot in the waveguide determines the current flow. Thus, the position determines the impedance presented to the transmission line and the amount of energy coupled to the slot and radiated from the slot.

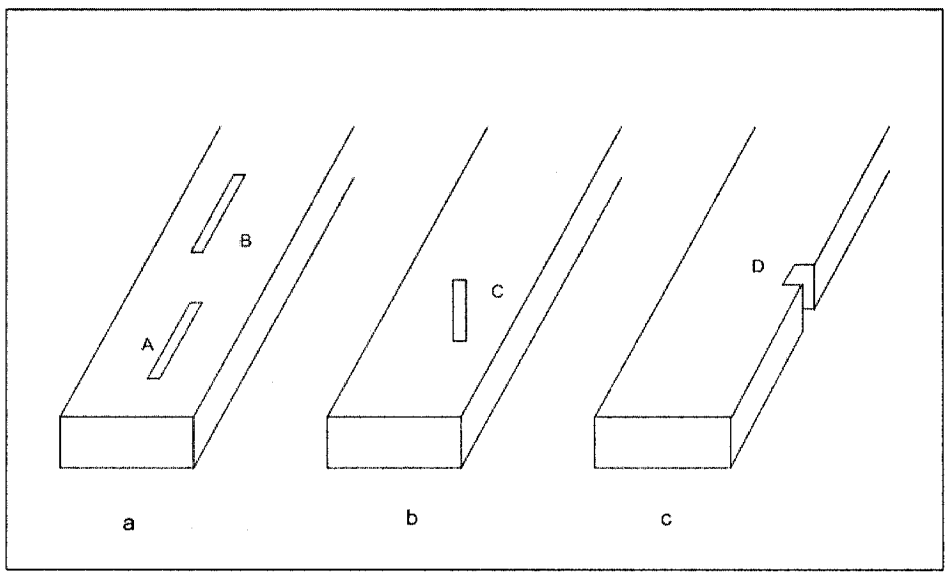

Figure 3.3: (a) Longitudinal broad wall slots (b) Inclined broad wall slot

(c) Inclined narrow wall slot.

The current in the walls of the guide must be proportional to the difference in electric field between any two points. Therefore, a slot in the exact center of the broad wall of the waveguide (slot A) will be essentially non radiative, since the electric field is symmetrical around the center of the guide and thus is identical at both edges of the slot. It can be used to measure the fields within the guide (VSWR indicator) with an inserted movable probe.

As the slot is positioned away from the centerline (slot B), the difference in field intensity between the edges of the slot is larger, so that more current is interrupted and

more energy is coupled to the slot, increasing radiated power. The induced electric field in slot B is increased by increasing the offset; the polarity of the induced electric field is reversed by reversing the direction of the offset.

As the sides of the waveguide are approached, the field is very small, since the sidewalls are short circuits for the electric field. The induced current must also be small; longitudinal slots very close to the sidewalls will not radiate significantly.

Slot C, which is inclined or tilted, primarily interrupts longitudinal current. The induced electric field in slot C is increased by increasing the tilt. The polarity of the induced electric field is reversed by reversing the direction of the tilt.

Finally for slot D, the inclination causes interruption of the transverse current in the narrow wall, the more the inclination, the greater the interruption. The polarity of the induced electric field is reversed by reversing the direction of the inclination.

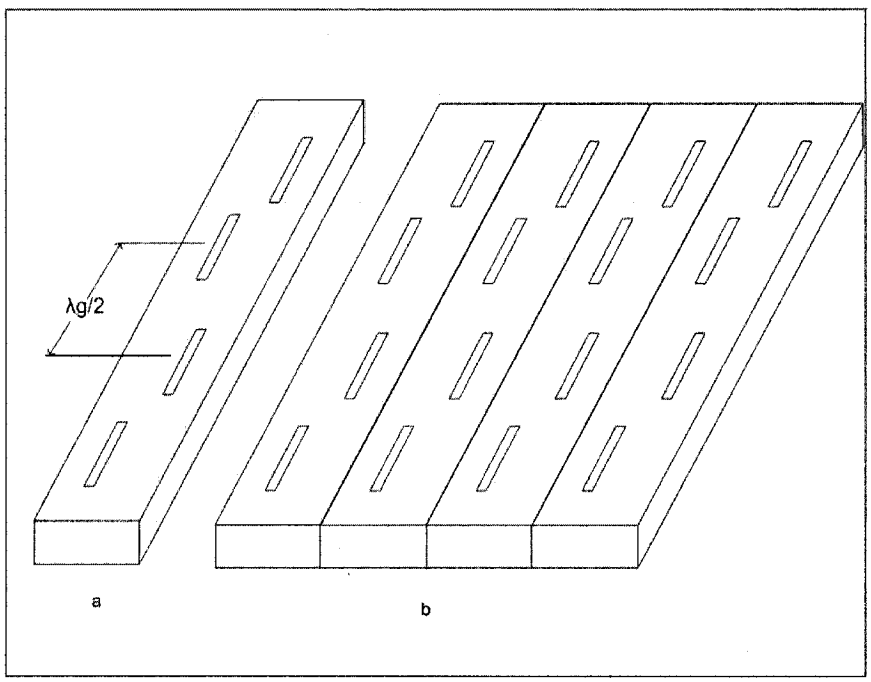

Figure 3.4: Array of longitudinal slots; (a) linear array

(b) planar array.

A desirable feature shared by all of these radiating-type slots (Figure 3.3) is that there is mechanical control over the amount of radiation, through choice of the amount of displacement or inclination.

In Figure 3.4 are shown slots that are placed $\lambda_g / 2$ apart and alternately offset where λ_g is the guide wavelength for the TE_{10} mode. Figure 3.4 (a) is an example of a linear array for which the induced electric fields in the various slots will have a common phase and an arbitrary amplitude distribution. Linear arrays of this type can produce a useful antenna pattern consisting of a main beam and side lobes of governed heights. In Figure 3.4 (b), linear arrays are placed side by side to produce a planar slot array. By controlling the relative excitation of the individual linear arrays, one is able to achieve a governable two-dimensional aperture distribution and thereby produce a desired pattern.

The array is said to be standing-wave fed when the slots are placed $\lambda_g / 2$ apart in a common waveguide. If the spacing is other than $\lambda_g / 2$, array is said to be travelling-wave fed. These definitions will be elaborated in Chapter 4.

3.4 Development of design equations for a slot array

Three design equations necessary for a slotted array antenna on the broad wall of a dielectric-filled waveguide will be developed and discussed starting with the $\vec{E}$-field distribution induced in the slot (Section 3.4.1). It can be obtained by modeling the actual situation with a 'zero' wall thickness and applying boundary condition for tangential magnetic field, $\vec{H}$ at all points in the slot aperture. In the development process, concepts of self-admittance, active admittance, slot voltage, mode voltage

and their relation and analytical formulation of mutual coupling will be presented and input matching taken into consideration.

3.4.1 The electric field distribution in a longitudinal slot

The design of a linear array begins with an understanding of the $\vec{E}$-field distribution in the aperture of a single longitudinal slot when it is excited by a TE_{10} mode. The slot in Figure 3.5 is assumed to be followed by a matched load and to be fed by a matched generator. The source is a TE_{10} mode traveling in the $+z$ direction. The slot is cut in the upper broad wall of the rectangular waveguide and the wall is assumed to be embedded in a large ground plane of good conductivity. The slot is offset a distance x_0 from the side wall and it has a length $2l$, a width w.

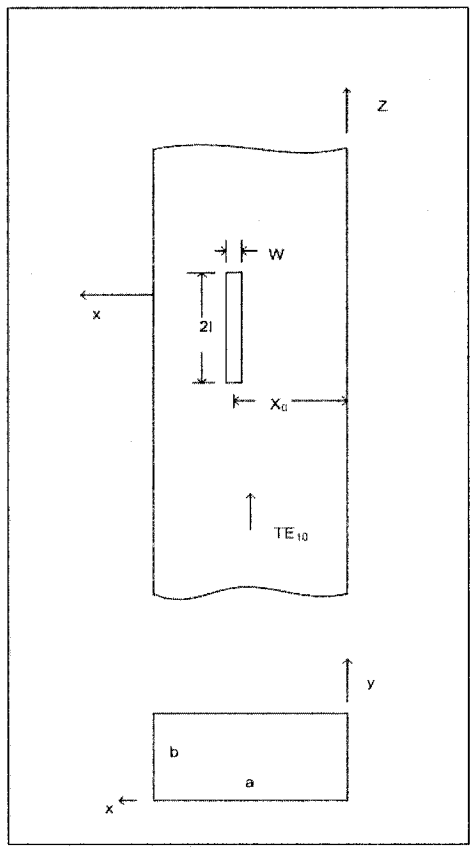

Figure 3.5: A single longitudinal slot excited by a TE_{10} mode.

When the waveguide walls are very thin (a modern trend), the $\vec{E}$-field distribution induced in the slot can be known by taking the wall of 'zero' thickness and applying the boundary condition that is matching internal and external expressions for tangential $\vec{H}$ at all points P in the slot aperture. In mathematical terms

$$\hat{1}_y \times [\vec{H}^{inc}_{\text{int}}(P) + \vec{H}^{scat}_{\text{int}}(P)] = \hat{1}_y \times \vec{H}^{ext}(P) \tag{3.6}$$

where $\hat{1}_y$ is a unit vector normal to the slot surface, $\vec{H}^{inc}_{\text{int}}$ is the incident field of TE_{10} mode, $\vec{H}^{scat}_{\text{int}}$ is the field scattered by the slot into the waveguide, and $\vec{H}^{ext}$ is the field scattered by the slot into the outer half-space.

Using Stevenson's Green's functions for the internal scattered field and Green's functions for a half space, equation (3.6) can be written in the component form as

$$\int_{slot} [G_{xx}(P,P')E_x(P') + G_{xz}(P,P')E_z(P')]\, dS' = -\frac{\beta_{10}}{\pi/a} A_{10} \sin(\frac{\pi x}{a}) e^{-j\beta_{10}z} \tag{3.7}$$

$$\int_{slot} [G_{zx}(P,P')E_x(P') + G_{zz}(P,P')E_z(P')]\, dS' = jA_{10} \cos(\frac{\pi x}{a}) e^{-j\beta_{10}z} \tag{3.8}$$

in which $P(x,z)$ is any observation point in the slot aperture and $P'(x',z')$ is any source point in the slot aperture; $k = \omega(\mu_0\varepsilon)^{1/2}$ is the wave number, ε is permittivity of the dielectric filling the waveguide, $\beta_{10} = [k^2 - (\pi/a)^2]^{1/2}$ the propagation constant of the TE_{10} mode. A Method of Moments type of solution can yield approximations to $E_x(P')$ and $E_z(P')$. When $w<<l$, which is the usual case, one finds that $E_z(P')$ is

negligible compared with $E_x(P')$. The problem is then considerably simplified and equation (3.8) becomes

$$\int_{slot} G_{zx}(P,P')E_x(P')\ dx'dz' = jA_{10}\cos(\frac{\pi x}{a})e^{-j\beta_{10}z} \tag{3.9}$$

where

$$G_{zx}(P,P') = \frac{1}{2\pi j\omega\mu_0}(\frac{\partial^2}{\partial z'^2}+k_0^2)\frac{e^{-jk_0R}}{R} + \frac{2}{j\omega\mu_0 ab}\sum_{m=0}^{\infty}\sum_{n=0}^{\infty}\frac{\varepsilon^2_{mn}}{\gamma_{mn}}\cos(\frac{m\pi x}{a})\cos(\frac{m\pi x'}{a})$$
$$\times(\frac{\partial^2}{\partial z^2}+k^2)e^{-\gamma_{mn}|z-z'|} \tag{3.10}$$

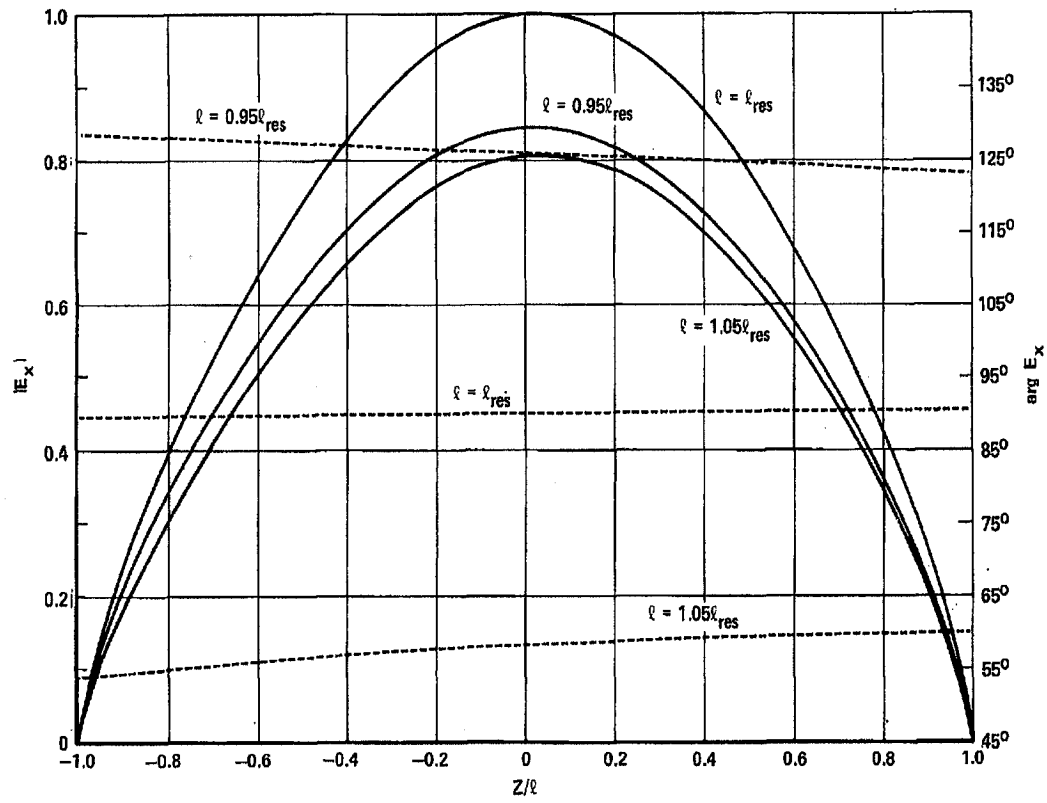

Figure 3.6: Electric field distribution versus length for a longitudinal shunt slot; solid lines, magnitude; dashed lines, phase ([1]).

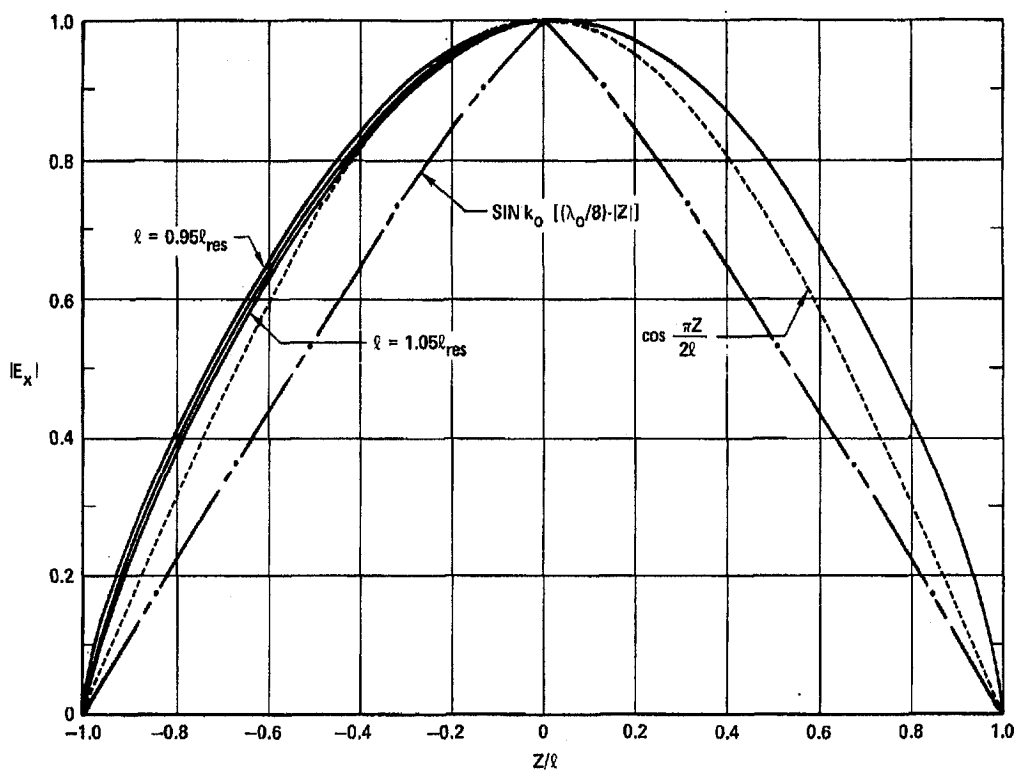

Figure 3.7: Normalized electric field magnitude versus length for a longitudinal shunt slot. Comparison to cosinusoidal distribution ([1]).

where $R = \overline{PP'}$ and k_0 is the free-space wave number. The propagation constant γ_{mn} of the mn th mode is given by $\gamma_{mn} = [(\frac{m\pi}{a})^2 + (\frac{n\pi}{b})^2 - k^2]^{1/2}$ and the Neumann numbers $\varepsilon_{mn}^{\ 2}$ are such that $\varepsilon_{00}^{\ 2} = 1/4$, $\varepsilon_{0n}^{\ 2} = \varepsilon_{m0}^{\ 2} = 1/2$, $\varepsilon_{mn}^{\ 2} = 1$ otherwise.

The various curves in Figure 3.6 show typical results and give the magnitude and phase of E_x for an isolated slot where l_{res} is the resonant length of the slot. The slot is on broad wall of an air-filed *X*-band waveguide *(a* = 0.900 inch, *b* = 0.400 inch). The slot offset is 0.120 inch. The frequency used is 9.375 GHz. The distributions for three slot lengths are displayed.

It is seen that the amplitude distribution is almost symmetrical for all three lengths, being greatest at resonance, and that the phase distribution is most nearly uniform at

resonance. Phase distribution is also more or less uniform even at lengths 5 percent above and below resonance. If all three amplitude distributions are normalized to unity, the result is as shown in Figure 3.7. For this range of slot lengths, amplitude distribution is fairly constant, the level being slightly affected by length. A plot of half-cosinusoid shows that the actual field distribution is somewhat broader, but not dramatically so. Similar results have been obtained for other slot offsets, for other waveguide sizes and frequencies, and for other dielectrics than air filing the guide. The important conclusion can be drawn is that the electric field distribution along the centerline of a narrow longitudinal slot when within 5 percent of resonance and when excited by TE_{10} mode can be represented as

$$E_x = \frac{V^s}{w}\cos(\frac{\pi z'}{2l}) \tag{3.11}$$

in which V^s is the slot voltage, measured across the slot at its center. In equation (3.11), the z' origin has been taken in the waveguide cross section which bisects the slot. Equation (3.11) can be contrasted to the assumption in the earlier theory [11]

$$E_x = \frac{V^s}{w}\sin[k_0(l-|z'|)]. \tag{3.12}$$

The resonant length of a shunt slot is affected by the permittivity of the dielectric filling the guide. For a dielectric-filled guide, equation (3.11) is clearly superior. Figure 3.7 also contains a normalized plot of equation (3.12) for the case of a dielectric of high enough permittivity to cause the resonant length to be $\lambda_0/4$. Equation (3.11) is taken as a more realistic approximation than equation (3.12) to the true field distribution in the slot under all circumstances.

The slot voltage V^s is given by

$$V^s = \int_{x_0-w/2}^{x_0+w/2} E_x(x',0)dx'. \tag{3.13}$$

3.4.2 Normalized admittance calculation based on amplitude distribution

When the assumption is made that the electric field distribution in a longitudinal slot is given by equation (3.11), the internal field in the dominant mode can be related to slot voltage, in the form [1]

$$B_{10} = C_{10} = -Kf(x,l)V^s \tag{3.14}$$

in which B_{10} and C_{10} are, respectively, the complex amplitudes of the back and forward scattered TE_{10} modes. The constant K and the function $f(x,l)$ are given by

$$K = \frac{2(\pi/a)^2}{j\omega\mu_0(\beta_{10}/k)(ka)(kb)} \tag{3.15}$$

$$f(x,l) = \frac{(\pi/2kl)\cos(\beta_{10}l)}{(\pi/2kl)^2 - (\beta_{10}/k)^2}\sin(\frac{\pi x}{a}). \tag{3.16}$$

Slot offset, x is measured from the center line of the broadwall of the waveguide. If there are N slots in an array, for the n^{th} slot, the cause of slot voltage V^s are TE_{10} modes passing underneath the slot in both directions plus external coupling to the other $N-1$ slots in the array.

It is first useful to introduce the concept of an equivalent circuit for the n^{th} slot. Equation (3.11) embodies the assumption that the electric field distribution in the slot is symmetrical. This symmetrical scattering can be modeled by a shunt admittance of an equivalent lossless transmission line [6] for which

$$B_n = C_n = -\frac{1}{2}\frac{Y_n^a}{G_0}V_n \tag{3.17}$$

Where Y_n^a is the active admittance of the n^{th} slot (including mutual coupling).The term V_n is the mode voltage on the equivalent transmission line at the site of Y_n^a; G_0 is the characteristic conductance of the equivalent transmission line.

Equations (3.14) and (3.17) can be connected by requiring that B_{10} and B have the same phase at any cross section z and that the backscattered power levels be the same in both cases. Under those conditions, the two equations combine to give

$$\frac{Y_n^a}{G_0} = K_1 f_n \frac{V_n^s}{V_n} \tag{3.18}$$

in which $K_1 = \frac{1}{j(a/\lambda)}\sqrt{\frac{2(k/k_0)}{\eta G_0(\beta_{10}/k)(ka)(kb)}}$

with η the impedance of free space, and with

$$f_n = \frac{(\pi/2kl_n)\cos\beta_{10}l_n}{(\pi/2kl_n)^2 - (\beta_{10}/k)^2}\sin(\frac{\pi x_n}{a}). \tag{3.19}$$

For two different slots p and n, equation (3.18) can be written in ratio form as

$$\frac{Y_p^a/G_0}{Y_n^a/G_0} = \frac{f_p}{f_n}\frac{V_p^s}{V_n^s}\frac{V_n}{V_p}. \tag{3.20}$$

3.4.3 Relation between normalized admittance and mutual coupling

The causes of the slot voltage induced in the n^{th} slot should be investigated. The first cause is a TE_{10} mode of complex amplitude A_{10}, incident from the left $(z=-\infty)$. Assume that there is no other slot in the waveguide that precedes the n^{th} slot, and the waveguide is terminated beyond the n^{th} slot in a matched load, so the equivalent

transmission line circuit consists of the self admittance Y of the slot in parallel with the conductance of the transmission line G_0. The incident wave A on the transmission line causes a backscattered wave B, the two being related by

$$\frac{Y}{G_0} = -\frac{2(B/A)}{1+B/A} \tag{3.21}$$

This equation is equally valid if (B_{10}^n / A_{10}^n) is substituted for (B/A). So by rearrangement

$$B_{10}^n = -\frac{\frac{Y}{G_0}(x_n, l_n)}{2+\frac{Y}{G_0}(x_n, l_n)} A_{10}^n \tag{3.22}$$

Now equation (3.21) equally applies for a TE_{10} mode of complex amplitude D_{10}^n that is incident from the right $(z=+\infty)$. Then A_{10}^n will be replaced by D_{10}^n. Thus the scattering matrix of an isolated shunt slot, viewed as a two-port microwave device, is completely determined if $\frac{Y}{G_0}(x_n, l_n)$ is known. The total slot voltage is composed of four parts, i.e.,

$$V_n^s = V_{n,1}^s + V_{n,2}^s + V_{n,3}^s + V_{n,4}^s \tag{3.23}$$

in which $V_{n,1}^S$, is due to A_{10}^n, $V_{n,2}^S$ is due to D_{10}^n, $V_{n,3}^S$ is due to external mutual coupling with the other $N-1$ slots in the array and $V_{n,4}^S$ is due to internal mutual coupling. Elliott and Loughlin [2] found that in a waveguide of reduced height, the resonant length increases. This means that the tip-to-tip distance between successive slots in the same waveguide is less, indicating that the higher order modes scattered off one slot are less attenuated when they reach the neighboring slot. Their study revealed that internal higher order mode coupling consists solely of TE_{20}

contributions. The fourth part, $V_{n,4}^{S}$ is due to TE_{20} modes scattered off the $(n-1)^{st}$ and $(n+1)^{st}$ slots and incident on the n^{th} slot. Using equations (3.14), (3.19), and (3.22), we find that

$$V_{n,1}^{s} = \frac{1}{Kf(x_n, l_n)} \frac{Y(x_n, l_n)/G_0}{2 + Y(x_n, l_n)/G_0} A_{10}^{n} \tag{3.24}$$

Similarly,

$$V_{n,2}^{s} = \frac{1}{Kf(x_n, l_n)} \frac{Y(x_n, l_n)/G_0}{2 + Y(x_n, l_n)/G_0} D_{10}^{n} \tag{3.25}$$

It was analytically shown in [2] through the application of the reciprocity theorem that the sum of two parts of slot voltages that are due to external and internal mutual coupling is

$$V_{n,3}^{s} + V_{n,4}^{s} = \frac{1}{f_n^2} \frac{Y(x_n, l_n)/G_0}{2 + Y(x_n, l_n)/G_0} \{-j(\beta_{10}/k)(k_0 b)(a/\lambda)^3 \cdot \sum_{m=1}^{N}{}' V_m^S g_{mn} - j\frac{(\beta_{10}/k)}{(\gamma_{20}/k)} e^{-(\gamma_{20}/k)kd} [h_n h_{n-1} V_{n-1}^S + h_n h_{+-1} V_{n+1}^S] \tag{3.26}$$

Where

$$\gamma_{20} = \sqrt{(2\pi/a)^2 - k^2} \tag{3.27}$$

$$g_{mn} = \int_{-k_0 l_m}^{k_0 l_m} \cos\left(\frac{z_m'}{4l_m/\lambda_0}\right) \left\{ \frac{1}{4l_n/\lambda_0} \left[\frac{e^{-jk_0 R_1}}{k_0 R_1} + \frac{e^{-jk_0 R_2}}{k_0 R_2}\right] + \left[1 - \frac{1}{(4l_n/\lambda_0)^2}\right] \int_{-k_0 l_n}^{k_0 l_n} \cos\left(\frac{z_n'}{4l_n/\lambda_0}\right) \frac{e^{-jk_0 R}}{k_0 R} dz_n' \right\} dz_m' \tag{3.28}$$

$$h(x,l) = 2\frac{(\lambda/4l)\cosh\left(\frac{\gamma_{20}}{k} kl\right)}{\left(\frac{\gamma_{20}}{k}\right)^2 + \left(\frac{\lambda}{4l}\right)^2} \cos\left(\frac{2\pi x}{a}\right) \tag{3.29}$$

In equation (3.26), the prime on the summation sign means that the term $m=n$ is to be excluded. In equation (3.28), the substitute variable $z = k_0\zeta$ has been introduced. R is the distance from the point $P_m(0,0,\zeta_m')$, measured in local coordinates at the m^{th} slot, to the point $P_n(0,0,\zeta_n')$, measured in local coordinates at the m^{th} slot. R_1 is the distance from P_m to $P_{n,1}(0,0,l_n)$ and R_2 is the distance from P_m to $P_{n,2}(0,0,-l_n)$. The variable distances R, R_1 and R_2 are shown in Figure 3.8.

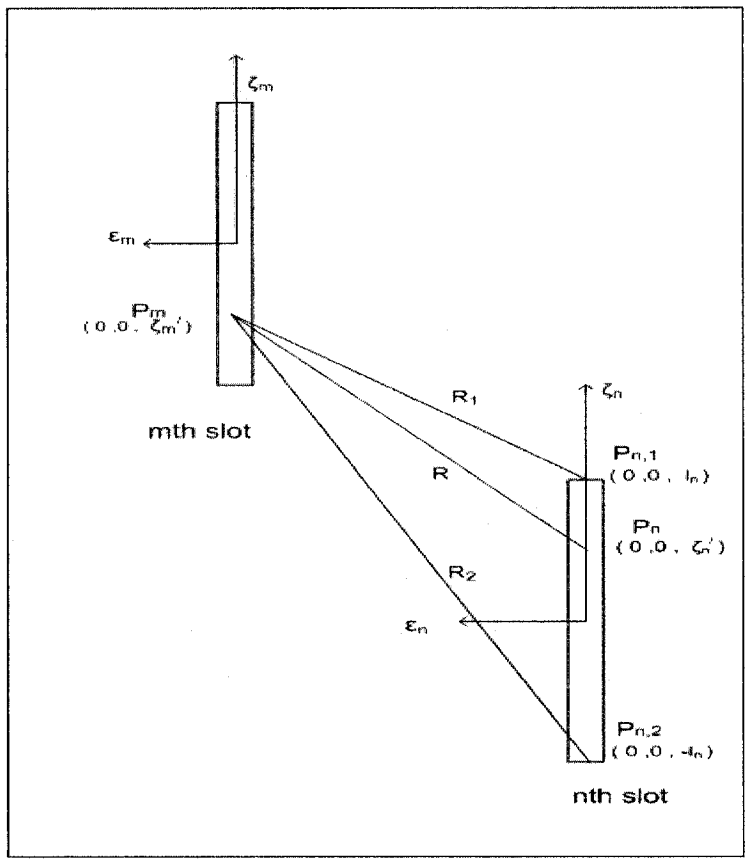

Figure 3.8: Geometry for mutual coupling calculation.

With the external and internal mutual coupling terms found in equation (3.26) for an array of waveguide-fed longitudinal shunt slots, expressions for the four partial slot voltages are now known.

For a resonantly spaced array (slots $\lambda_g/2$ on centers in a common waveguide) we have for the n^{th} slot [36]

$$\sum_{i=n}^{M} \frac{Y_i^a}{G_0} = \frac{A_{10}^n - (B_{10}^n + D_{10}^n)}{A_{10}^n + (B_{10}^n + D_{10}^n)}, \sum_{i=n+1}^{M} \frac{Y_i^a}{G_0} = \frac{(A_{10}^n + C_{10}^n) - D_{10}^n}{(A_{10}^n + C_{10}^n) + D_{10}^n} \tag{3.30}$$

in which $\frac{Y_i^a}{G_0}$ is the active admittance of the i^{th} slot, there being M slots in the waveguide which contains the n^{th} slot. The difference of the two expressions in equation (3.30) yields

$$\begin{aligned} \frac{Y_n^a}{G_0} &= \frac{A_{10}^n - (B_{10}^n + D_{10}^n)}{A_{10}^n + (B_{10}^n + D_{10}^n)} - \frac{(A_{10}^n + C_{10}^n) - D_{10}^n}{(A_{10}^n + C_{10}^n) + D_{10}^n} \\ &= -\frac{2B_{10}^n}{A_{10}^n + B_{10}^n + D_{10}^n} \end{aligned} \tag{3.31}$$

since $B_{10}^n \approx C_{10}^n$, if we use equation (3.14), equation (3.23), equation (3.24) and equation (3.25) to make substitutions in equation (3.31), rearrangement gives

$$\frac{Y_n^a}{G_0} = \frac{2f_n^2(x_n, l_n)}{\frac{2f_n^2(x_n, l_n)}{Y(x_n, l_n)/G_0} + MC_n} \tag{3.32}$$

where

$$\begin{aligned} MC_n = {} & j(\beta_{10}/k)(k_0 b)(a/\lambda)^3 \cdot {\sum_{m=1}^{N}}' \frac{V_m^S}{V_n^S} g_{mn}(x_m, l_m, x_n, l_n) \\ & + j\frac{(\beta_{10}/k)}{(\gamma_{20}/k)} e^{-(\gamma_{20}/k)kd} [h_n h_{n-1} \frac{V_{n-1}^S}{V_n^S} + h_n h_{+-1} \frac{V_{n+1}^S}{V_n^S}] \end{aligned} \tag{3.33}$$

Equation (3.32) along with equation (3.18) permits the design of shunt slot arrays in either dielectric-filled or air-filled waveguide, including external and internal mutual coupling.

3.4.4 Condition of input match

If there are M slots in the waveguide, the condition of input match is simply

$$\sum_{n=1}^{M} \frac{Y_n^a}{G_0} = \text{specific constant} \tag{3.34}$$

For a linear array the specific constant should be unity.

3.5 The methodology of design of a broadside linear array of resonantly spaced longitudinal slots (standing-wave feed)

If there are to be N slots spaced $\lambda_g/2$ apart, and a certain broadside pattern is desired with specific side lobe level, Chapter 5 describes the techniques to determine the slot voltage distribution V_n^s. Let it be assumed that this slot voltage distribution is known. When all the slots are in a common waveguide (which is the case for a linear array) and resonantly spaced ($\lambda_g/2$) at centers, the mode voltage V_n has a common value (except for an alternation in sign) for all slots. From equation (3.19), it can be seen that this alternation is compensated by an alternation in the direction of slot offset, which causes $\sin(\frac{\pi x_n}{a})$ to change sign at successive slots. For a broadside pattern, the slot voltage V_n^s will have same phase for slots. Then equation (3.18) indicates

that all the active admittances $\frac{Y_n^a}{G_0}$ should have the same phase. In such circumstances, the usual choice is to make $\frac{Y_n^a}{G_0}$ pure real for all n.

To use design equation (3.32) of Section 3.4.3, one needs first to express in functional form the input data of self-admittance, $\frac{Y}{G_0}$ for an isolated slot as a function of its length and offset. That data can be obtained in several ways.

(1) Experimentally, by constructing a family of waveguides, each with single a slot but with different offsets and shorter-than-resonant lengths. After $\frac{Y}{G_0}$ has been measured for each member of the family, the slots can be lengthened and the measurements repeated, etc. For most applications it is sufficient to obtain data in the range $0.95l_r \le l \le 1.05l_r$ where l_r is the resonant length and seven well-spaced data points per family member are usually sufficient [37].

(2) Computationally, using numerical technique like the Method of Moments [38] or FDTD [26].

(3) Scaling some known measured data like that of Stegen [6]. This method requires scaling the complete waveguide - including the wall thickness and the size of the slots [39].

(4) By using commercially available simulation software [10], [40] for the equivalent circuit of a longitudinal slot.

For this thesis, a Finite Element Method based commercial software package, Ansoft HFSS [3] has been used to generate $\frac{Y}{G_0}$ curves as a function of slot length and offset.

R.J. Stegen [6] has found that the admittance data of an isolated slot can be presented in a universal form that is extremely useful for computational purposes. To follow his

method with Elliot's design procedure; one should find that the input data can be normalized in the following way. Let

$$g(x) = \frac{G_r(x, l_r)}{G_0} \tag{3.35}$$

$$v(x) = kl_r(x) \tag{3.36}$$

$$y = l / l_r \tag{3.37}$$

$$h_1(y) = \frac{G(x,y)/G_0}{g(x)} \tag{3.38}$$

$$h_2(y) = \frac{B(x,y)/G_0}{g(x)} \tag{3.39}$$

$$h(y) = h_1(y) + jh_2(y). \tag{3.40}$$

The function $g(x)$ gives the conductance of a resonant-length slot versus offset. The function $v(x)$ is seen to be the resonant length versus offset multiplied by the wave number. The function $h(y)$ is a complex function such that

$$\frac{Y(x,l)}{G_0} = g(x)h(y). \tag{3.41}$$

The two components of $h(y)$ are real functions, with $h_1(y)$ representing $\frac{G(x,y)}{G_0}$ in ratio to $g(x)$ and $h_2(y)$ similarly representing $\frac{B(x,y)}{G_0}$ in ratio to $g(x)$. The virtue of assembling the data in this form, with $\frac{Y}{G_0}$ normalized to $g(x)$, is that when the data are plotted versus $y = l/l_r$, the result is found to be essentially independent of offset. Since $g(x)$, $v(x)$, $h_1(y)$ and $h_2(y)$ can all be fitted with a few terms of a polynomial, the representation of $\frac{Y}{G_0}$ in the form of equation (3.41) is helpful in the ensuing calculation.

With $\frac{Y}{G_0}$ now a known input function, the next step is to find the starting values for the lengths and offsets of all slots in the array. Since the design procedure converges rapidly, it would be sufficient to start with all the slots on the center-line and resonant length.

With these lengths and offsets, the next step is to calculate MC_n, the mutual coupling term from equation (3.33) for every value of n, using the desired slot voltage distribution $\frac{V_n^s}{V_m^s}$, known from pattern requirements.

With this information in hand, a computer search is to be performed to find a couplet (x_n, l_n), which will make the denominator of equation (3.32) pure real. What can be found is that there is a continuum of couplets (x_n, l_n) which will satisfy this condition Similarly, for the *pth* slot there is a continuum of couplets which will make the denominator of equation (3.32) pure real (with p replacing n). But for a given acceptable couplet (x_n, l_n), there is only one acceptable couplet (x_p, l_p) which will also satisfy the design equation (3.18) in ratio form, i.e., equation (3.20).

Thus for each acceptable couplet (x_n, l_n), there is a set of acceptable couplets, one couplet for each slot in the array, which makes each active admittance pure real and also satisfies the design equation (3.18).

Of all these sets, the proper one to choose is the one which causes the sum of the normalized active admittances to be unity since this the condition for an input match by equation (3.34).

This procedure must be iterated because the chosen family of couplets will undoubtedly not agree with the original guess for slot lengths and offsets. One needs

to recompute MC_n from equation (3.33) with new (x_n, l_n) values keep cycling through this procedure until the last set of values becomes very close to the immediate previous set. At this point the design of the array of longitudinal slots is complete. For this thesis, the commercial software, MATLAB was used for coding the design algorithm.

Chapter 4

Numerical results I: Single slot on broadwall of an SIW

4.1 Introduction

This chapter mainly deals with the impedance properties of an isolated slot. The conversion of the SIW to its equivalent counterpart based on an established empirical relation has been discussed and the accuracy of this method has been investigated. Simulation software is used for generating admittance properties of the slot on broadwall of an SIW with a prior check of validity of this technique. From the self-admittance data thus generated, Stegen-type of curves are derived. These curves are then suitably polyfitted into expressions to be used in the array design.

4.2 Conversion from substrate integrated waveguide to an equivalent rectangular waveguide

The width of the equivalent broad wall of the rectangular waveguide, a_{RWG} is the key of the design procedure. A substrate integrated rectangular waveguide, SIW (often referred to SIRW) is composed of two parallel arrays of metallic via-holes, which delimit the waveguide TE_{10} wave propagation area. The propagation constant and the radiation loss depend on parameters a, p and d, which denote the width of the SIW, the period and the diameter of via holes, respectively (Figure 4.1 (a) and (b)).

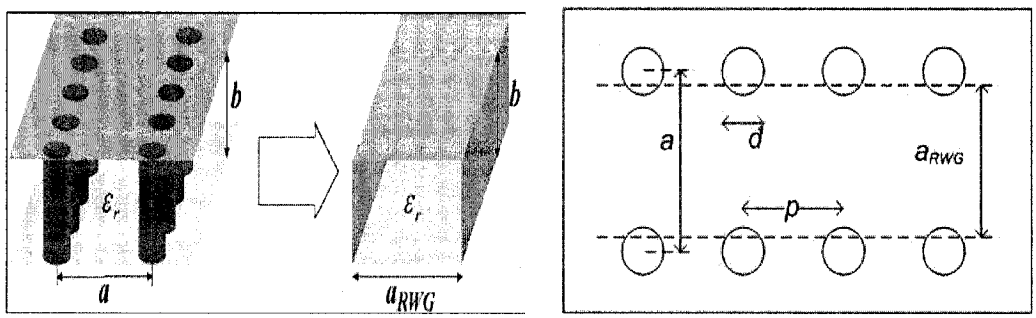

(a) (b)

Figure 4.1: (a) SIW and the equivalent rectangular waveguide [29]

(b) Topology of an SIW.

4.2.1 Selection criteria of via hole diameter and post pitch

In [23], parametric effects of d and p have been studied in detail in pursuit of making the synthesized waveguide section radiationless or free from leakage loss. It is notable that equations (3.1) and (3.2) do not depend on the thickness of the waveguide. The thickness only affects the Q-factor [23]. The propagation of TE_{10} mode is related to a so long the waveguide height, b is smaller than a. The parameters of via-holes d and p are set to minimize the radiation loss as well as return loss.

Deslandes *et al.* [23] have shown through simulation by HFSS [3] that the radiation loss is lower than 0.008 dB/wavelength for an electrically small post with $d < 0.2\lambda$ and a ratio of $d/p = 0.5$. They used a structure with parameters $a = 5.567\ mm$, $b = 0.508\ mm$ and $\varepsilon_r = 2.2$. The loss tends to decrease as the post gets smaller for a constant ratio of d/p. Post diameter affects the return loss of the waveguide

section as viewed at the input port. With $d / p = 0.5$, the choice of the via diameter must follow such a design rule as $d / a < 0.4$ [23].

4.2.2 Selection of a, d and p of our SIW :

Our goal is to design a linear array antenna at 30 GHz on an integrated waveguide with Rogers RT /Duroid 5880 substrate ($\varepsilon_r = 2.2$, loss tangent = 0.0009).

We chose,

- $a = 5.57\,mm$, same value as Deslandes *et al.* [21] used to design a wide-band microstrip transition at 28 GHz for SIW with Rogers RT /Duroid 5880 substrate. The SIW showed to have an operational bandwidth from 24 to 38 GHz including transition. The design frequency, 30 GHz falls roughly halfway within the band.
- $d / p = 0.5$, a typical value chosen for many designs with SIW [27], [29], [34], [40] etc.
- $d = 0.8\,mm$
- $b = 1.575\ mm$

4.2.3 The derivation of an equivalent rectangular waveguide

From Chapter 3, for design of slot array antenna on broadwall of an SIW, the design procedure of slot array antenna on broadwall of a dielectric-filled waveguide need to be followed; it is therefore necessary to find an equivalent waveguide having same dielectric constant as the SIW. A widely used and reliable practice is to convert the SIW to an equivalent rectangular waveguide by an empirical equation using simulation software like HFSS ([20], [21], [23] and [24]).

With selected parameters of the SIW from Section 3.2, an estimate of the cut-off frequencies of the first two dominant modes are calculated from equations (3.1) and (3.2) which are 19.627 GHz and 39.05 GHz respectively. The equivalent waveguide width, a_{RWG} as calculated from equation (3.3) is 5.149 mm which is supposed to have an error of order $\pm 5\%$, provided $p < \lambda_0 \cdot \sqrt{\varepsilon_r}/2$ and $p < 4d$ [20].

To get a more accurate a_{RWG}, three sections of SIW with $L_1 = 16\,mm$, $L_2 = 12.8\,mm$, $L_3 = 9.6\,mm$ were simulated. Ansoft HFSS [3] was used for this purpose. The results from simulations are as follows

$$\angle S^{L2}{}_{21} - \angle S^{L1}{}_{21} = 160^0$$

$$\angle S^{L3}{}_{21} - \angle S^{L1}{}_{21} = 256.13^0$$

$$\angle S^{L3}{}_{21} - \angle S^{L2}{}_{21} = 96.01^0$$

Using equation (3.4), we get

$$\beta^{L1,L2}{}_{SIW} = 698.13$$

$$\beta^{L1,L3}{}_{SIW} = 698.48$$

$$\beta^{L2,L3}{}_{SIW} = 698.24$$

So the average is $\beta_{SIW} = 698.28$.

With this average value of β_{SIW}, from equation (3.5), we get $a_{RWG} = 5.082\,mm$.

To compare the accuracy of the aforementioned conversion technique, the SIW with chosen value of parameters (a, p, d and b) was fed from both sides by rectangular waveguides having width, $a_{RWG} = 5.082\,mm$ and was simulated for a frequency range, 25 GHz to 35 GHz. The S-parameters were evaluated at the inputs of the SIW.

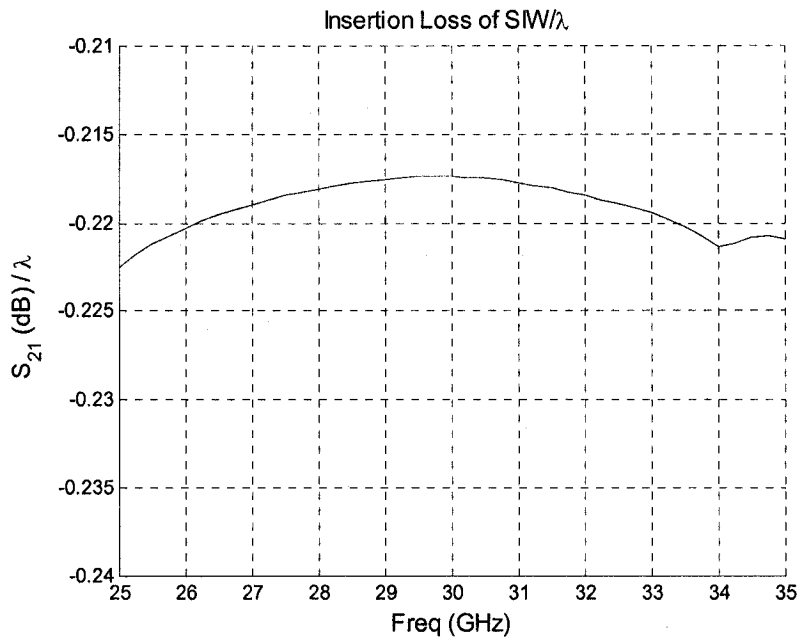

Figure 4.2: Insertion loss of SIW/ λ.

The negligible insertion loss per unit wavelength from 25 GHz to 35 GHz (Figure 4.2) of this SIW reinforces the fact that via holes with selected diameter and pitch are working as side walls of waveguide. In this calculation the conductor loss and dielectric loss have been ignored, so the loss solely comes from radiation.

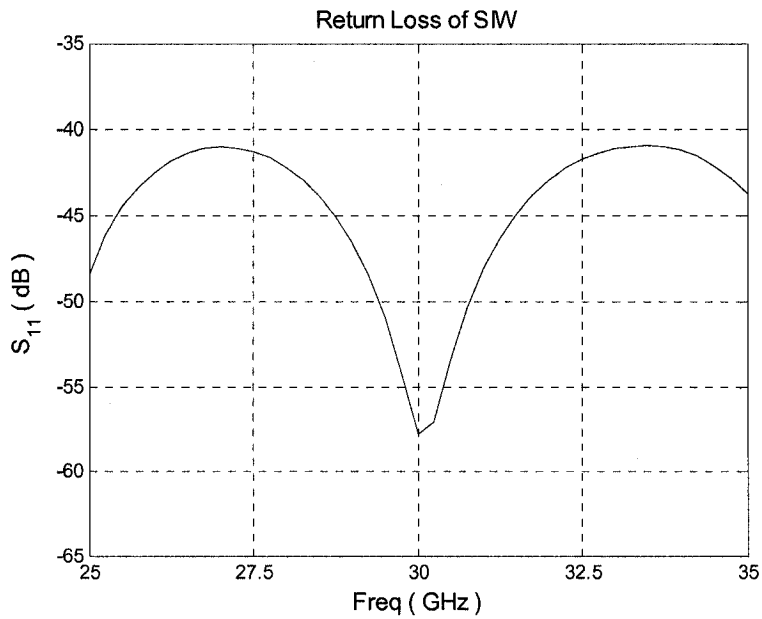

Figure 4.3: Return loss of SIW.

As shown in Figure 4.3, the return loss of the SIW remains below 40 dB in the frequency band from 25 GHz to 35 GHz with lowest value (~ -57 dB) at 30 GHz. From simulation point of view, this return loss indicates a very good match of characteristic impedance of equivalent waveguide with that of the SIW.

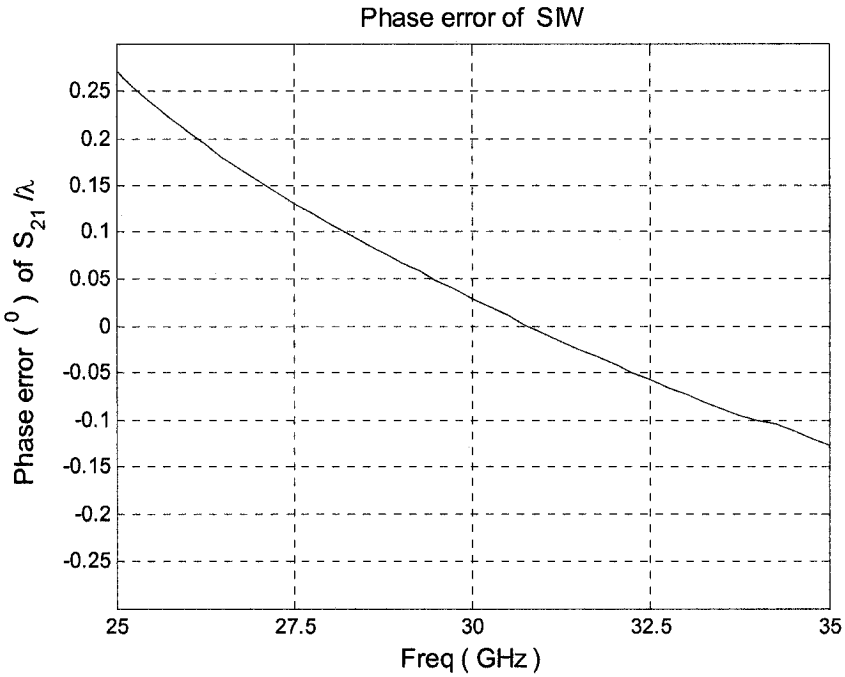

Figure 4.4: Phase error (degree) of S_{21}/λ.

The difference in phase of the transmission coefficients for the SIW and its equivalent waveguide shows a very close match (Figure 4.4) which indicates the equivalent waveguide has the same propagation constant as that of SIW.

4.3 Methodology of generating self-admittance curves and resonance characteristics of a single slot

Once the equivalent rectangular waveguide is derived from SIW, the next required job is to gather information of normalized self-admittance, $\frac{Y}{G_0}$ of a single slot on

broadwall of SIW as a function of slot length and displacement from center line of broadwall (offset).

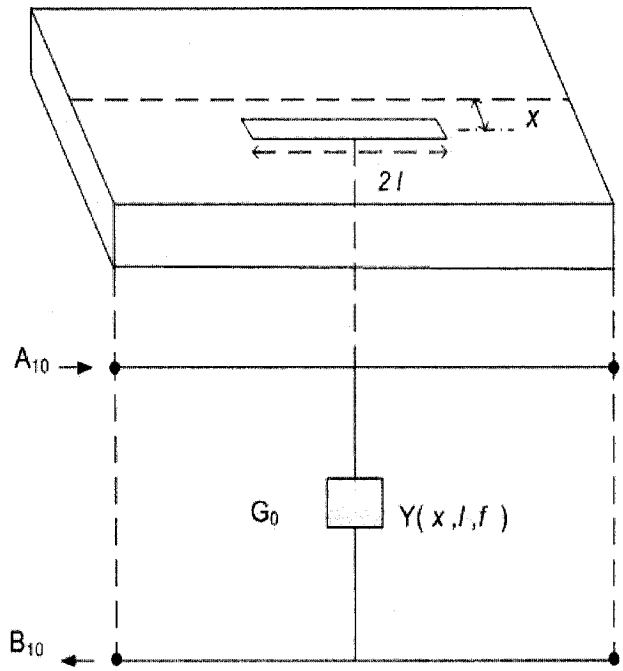

Figure 4.5: Longitudinal slot on broad wall of a rectangular waveguide and its equivalent circuit.

In the development of theory for a longitudinal slot in the broad wall of a waveguide, it has been shown that if a symmetrical *E*-field distribution is assumed to exist in the slot, the TE_{10} mode scattering is equivalent to the scattering caused by a shunt element in a two-wire transmission line (Figure 4.5). This is a good assumption if the slots are narrow (slot width << slot length) and if the slot offsets are not too large.

In many of the works with longitudinal slots on broadwall of a waveguide, this is a basic assumption [1], [11], [26], [38], [40] etc.

The obvious simplicity of the shunt element model is that if the reflection coefficient

for the fundamental TE_{10} mode of an isolated longitudinal slot can be determined, the equivalent normalized slot admittance is readily available from equation (4.1)

$$\frac{Y}{G_0} = \frac{-2\frac{B_{10}}{A_{10}}}{\frac{B_{10}}{A_{10}}+1} = \frac{-2S_{11}}{1+S_{11}}. \qquad (4.1)$$

As discussed in Chapter 3 (Section 3.5), several techniques have been used to gather the data for self-admittance of an isolated slot. Josefsson [38] used the Method of Moments technique to obtain the reflection coefficient of the fundamental mode and used equation (4.1) to generate $\frac{Y}{G_0}$ data. Theron and Cloete [39] simply translated Stegen's measurement data to a different frequency (38 GHz) including scaling of dimensions. Lu *et al.* [40] used shunt admittance for longitudinal slot in substrate integrated waveguide. They used the simulation software, Agilent MoM to generate scattering parameters. They later verified their Stegen-type data generated from comparison with measurement values.

For this thesis, the commercially available Finite Element Method based software package, Ansoft HFSS [3] has been utilized to model an isolated slot. The waveguide with width a_{RWG} was truncated at half guide-wavelength on both sides from the center of the slot. The assumption of a matched generator and load in theory for an isolated slot was realized by waveport excitation at both ends.

The shunt element is assumed to be lumped at the center of the slot (Figure 4.5) and the reflection is assumed to originate from this plane of discontinuity.

After simulation, data were post processed by transferring the reference plane at the center of the slot and reflection coefficient (S_{11}) was evaluated at this plane.

For a fixed frequency, the self admittance of the radiating slot is a function of slot offset, x and slot length, $2l$.

For an array design, it is sufficient to obtain data in the range, $0.95l_r \le l \le 1.05l_r$, ([11], [37]).

To generate Stegen–type data, these steps were followed:

- The slot was characterized at several lengths, keeping the slot offset constant.
- The slot was then characterized at several offsets, keeping the slot length constant.

  Data of $\frac{Y}{G_0}$ were generated for $0.90l_r \le l \le 1.10\,l_r$ and for a offset range from 0.2 mm to 1.1 mm at 0.1 mm interval.

4.4 Validation of the methodology by simulation

Many of the slot arrays designed so far have been for *X*-band operation. Stegen's measurement data can serve as a standard for comparison of admittance properties of an isolated slot for those cases. However Stegen's data are for rectangular slots with round-ends. And the waveguide obviously had finite wall thickness. In theory of design discussed in Chapter 3, these two factors have been ignored.

The convenient assumptions -zero wall thickness and square-end slots, are appropriate for the printed circuit fabrication [29].

If necessary, thickness of wall could be treated as a stub waveguide [7], [41]. Some empirical correction can also be imposed for round-end slots [7], [11]. As a result, resonant characteristics, especially resonant length, may vary significantly roughly by

4% [7]) for square-end slots and with zero wall thickness, even though frequency and other dimensions are kept same as those used by Stegen.

More recently, some analytical results using computational technique [8], [38] are now available for square-end slots and zero wall thickness. Computed admittance properties, using Ansoft HFSS [3] simulation, have been compared with those earlier results.

To check the validity of this methodology by simulation, an air-filled rectangular waveguide was simulated having same dimensions/parameters of [38]:

Waveguide broad wall width, a = 22.86 mm

waveguide narrow wall width, b = 10.16 mm

frequency, f = 9.375 GHz

slot width, w = 1.59 mm

wall thickness, t = 0 mm.

Simulation by parametric variation of length and offset takes a very long run-time. A limited range of offset, 2 mm to 7 mm at an interval 1 mm, has been studied.

To follow Stegen's factorization (Section 3.5) procedure, three characteristic curves are of principle interest.

- $v(x) = kl_r(x)$, which is resonant length multiplied by wave number as a function of offset, x. In most cases, it is presented in an alternative way - resonant length normalized by wavelength ($\frac{2l_r}{\lambda}$) as a function of offset.

- $g(x) = \frac{G_r}{G_0}$, which is normalized resonant conductance ($\frac{G_r}{G_0}$) as a function of offset.

- $h(y) = \frac{Y}{G_r} = \frac{G + jB}{G_r}$, which is admittance normalized by resonant conductance as a function of normalized length, y or $\frac{l}{l_r}$.

Figure 4.6 shows a comparison of resonant length normalized by wavelength as a function of offset obtained by HFSS [3] simulation with that obtained by Josefsson [38]. Josefsson used the Method of Moments with sinusoidal basis functions. The resonant-length points for the method followed, were extracted from each of $\frac{Y}{G_0}$ curve. The plot shows that simulation points closely track the computational curve with an error-margin less than 0.5 %.

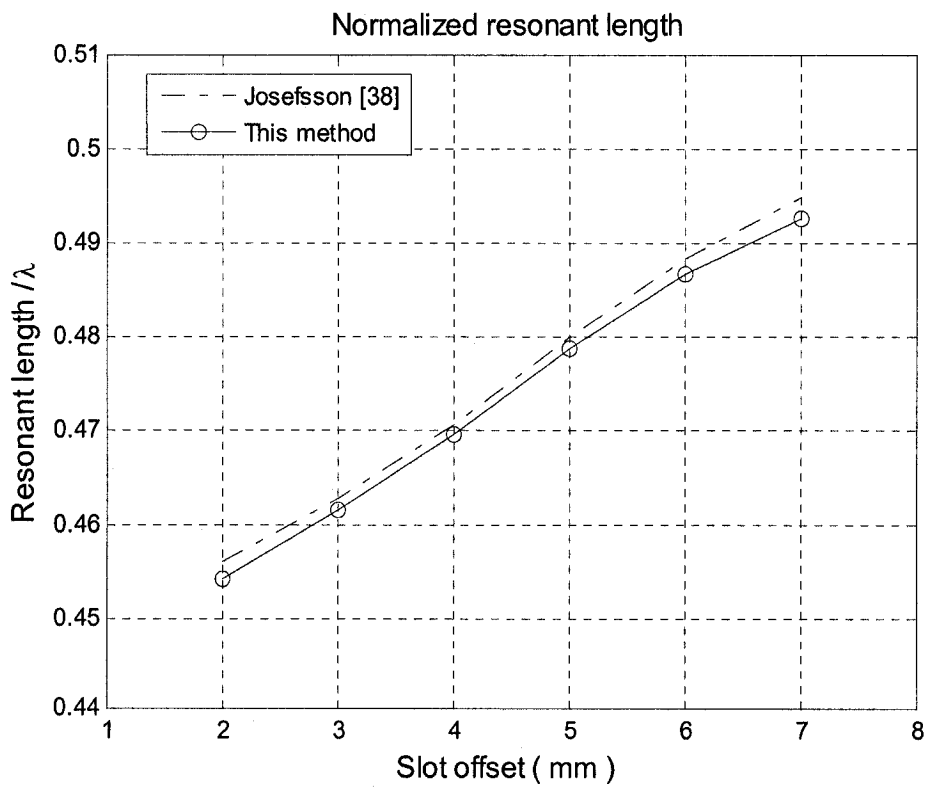

Figure 4.6: Comparison of resonant length.

However, in [38], the other two plots $-g(x)$ and $h(y)$ are not presented. $g(x)$, generated by simulation can be compared with that given by Stevenson's formula. Stevenson's formula for normalized resonant conductance for an air-filled waveguide, with the approximation of $kl \approx \frac{\pi}{2}$ is given [5] as

$$\frac{G_r}{G_0} = \left[2.09 \frac{\lambda_g}{\lambda} \frac{a}{b} \cos^2\left(\frac{\lambda}{\lambda_g} \frac{a}{b}\right) \right] \sin^2\left(\frac{\pi x}{a}\right) \tag{4.2}$$

Where, λ_g is the guide-wavelength and λ is the free-space wavelength. Stevenson's formula, applicable at resonance, is less accurate as the slot offset is increased [6]. Figure 4.7 shows this comparison. The same dimension and frequency as used by [38], were

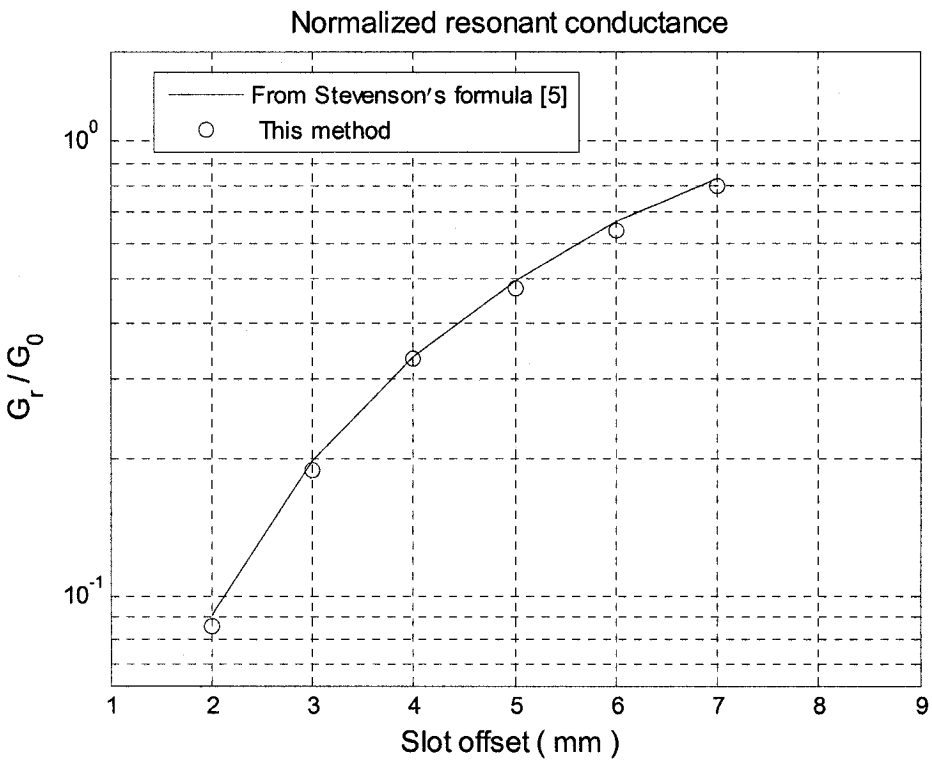

Figure 4.7: Comparison of resonant conductance as a function of offset.

used for Stevenson's formula. The plot shows a very close match between simulated points and the curve obtained from Stevenson's formula. Again these resonant conductance points were extracted from each of $\frac{Y}{G_0}$ curves.

A study of resonance characteristics presented in [26] and [40] for a dielectric–filled waveguide and for an SIW respectively reveals that because of dielectric filling, the normalized resonant length and normalized slot conductance exhibit stronger dependence on offset. In addition, the resonant conductance can no longer be represented by equation (4.2).

Finally $h(y)$ from simulation can be compared to that of Khac *et al.* [8] who show $h(y)$ at an offset of 4 mm. The only insignificant change in dimension is, in [8], $w = 1.5875\ mm$ which has been used in place of $w = 1.59\ mm$.

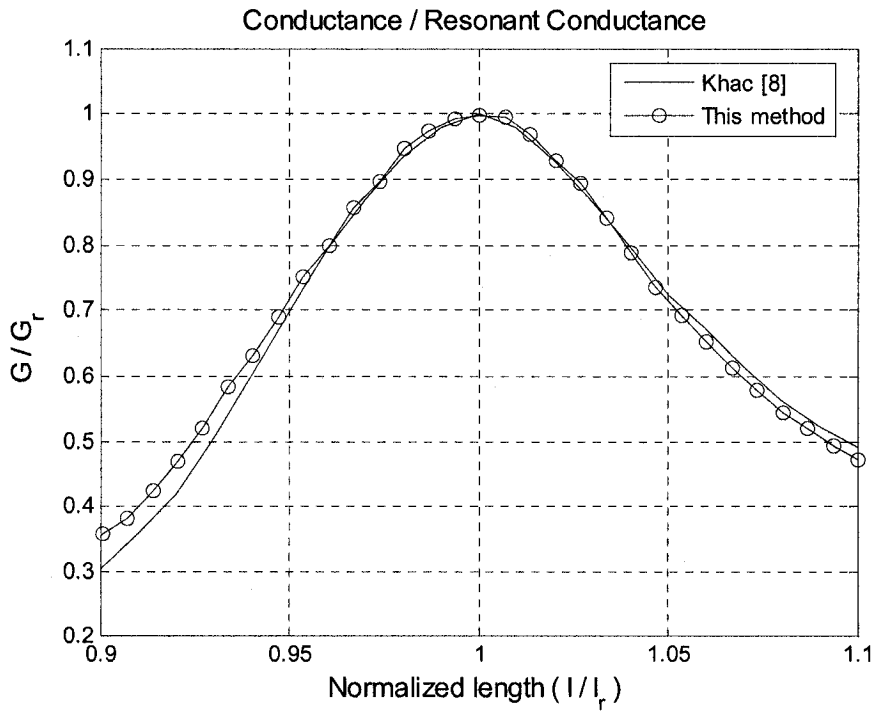

Figure 4.8: Simulated self-conductance versus normalized length; offset = 4 mm.

Figure 4.8 shows a comparison of $\frac{G}{G_r}$(real part of $h(y)$) as a function of y obtained by HFSS [3] simulation with that obtained from [8]. Figure 4.9 shows a comparison of $\frac{B}{G_r}$(imaginary part of $h(y)$) as a function of y obtained by HFSS [3] simulation with that obtained from [8].

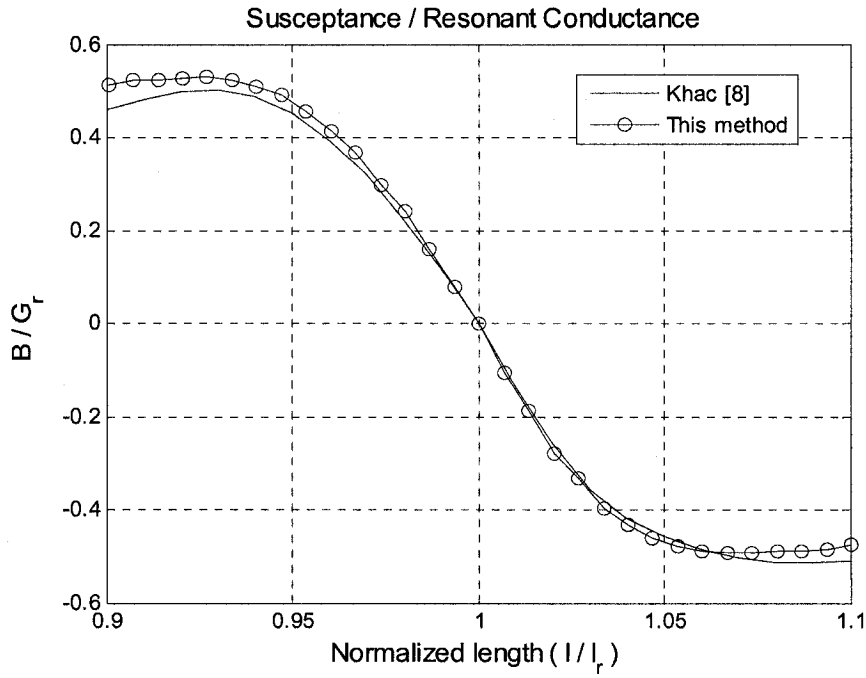

Figure 4.9: Simulated self-susceptance versus normalized length; offset = 4 mm.

All three sets of comparison for a single slot show a very good match between published results (computed data) and results generated by Ansoft HFSS [3].

4.5 Results of simulation for self-admittance curves and resonance characteristics of a single slot

The methodology outlined in Section 4.3 was followed in a meticulous and time consuming fashion to generate Stegen-type curves for a single slot on the broadwall

of our SIW. Data of $\frac{Y}{G_0}$ were generated for $0.90l_r \leq l \leq 1.10l_r$ and an offset range from 0.2 mm to 1.1 mm at 0.1 mm interval.

Figure 4.10 and Figure 4.11 show the $\frac{Y}{G_0}$ curves for two offsets 0.6 mm and 0.7 mm. The $\frac{Y}{G_0}$ curves at other offsets are similar in shape.

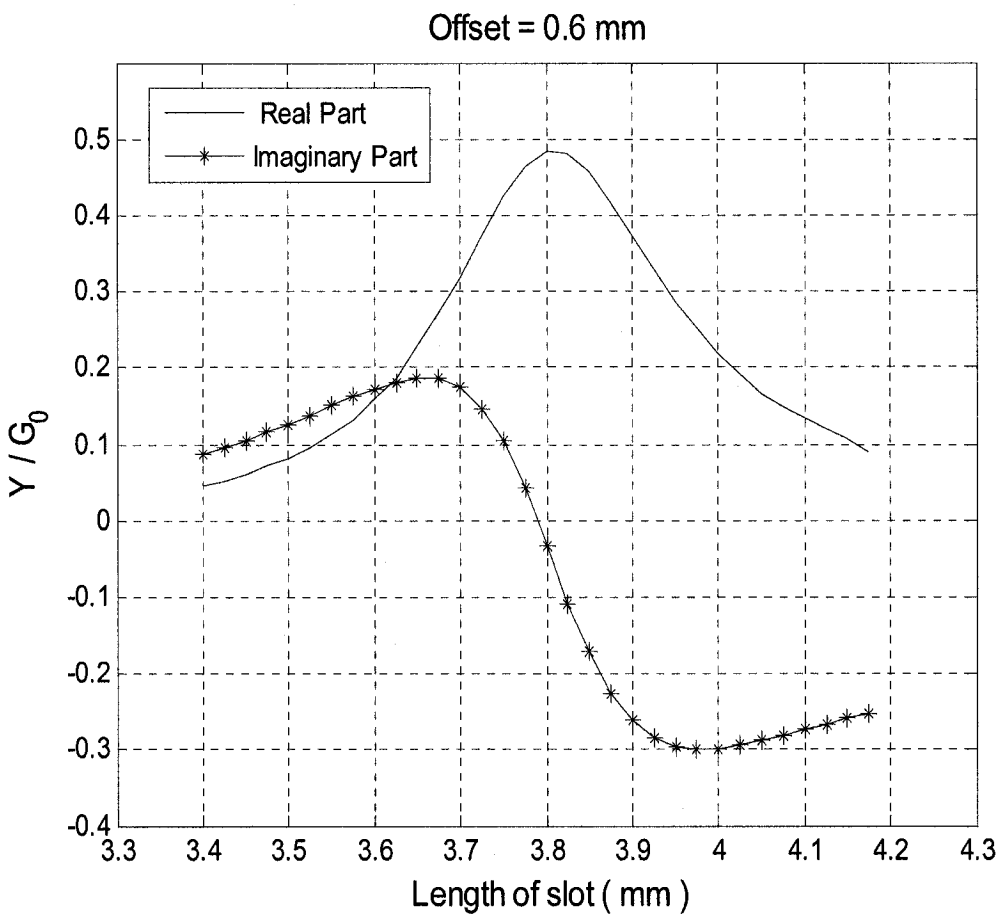

Figure 4.10: Self-admittance of the single slot at 0.6 mm offset.

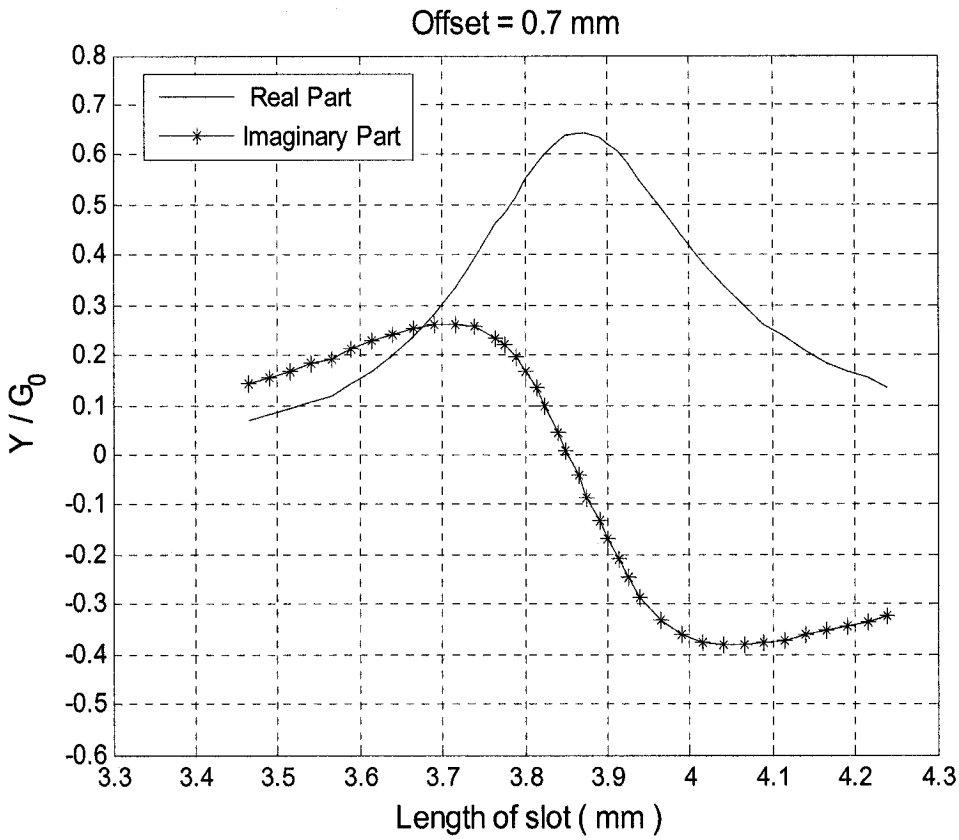

Figure 4.11: Self-admittance of the single slot at 0.7 mm offset.

Resonant length, l_r is the length at which the imaginary part of the admittance becomes zero. From each of the $\frac{Y}{G_0}$ curves, values of l_r can be found and these can be saved as a set. So the input, $v(x) = kl_r(x)$ as a function of offset is now known. Similarly, accumulation of normalized resonant conductance, $\frac{G_r}{G_0}$ from data at each offset, will produce the $g(x) = \frac{G_r(x, l_r)}{G_0}$ function. Therefore, functions, $h_1(y) = \frac{G(x,y)/G_0}{g(x)}$ and $h_2(y) = \frac{B(x,y)/G_0}{g(x)}$ can be generated and finally $\frac{Y(x,l)}{G_0}$ can

be replaced by a product term $\frac{Y(x,l)}{G_0} = \frac{G_r(x,l_r)}{G_0}\frac{G+jB}{G_r} = g(x)h(y)$ in design equation (3.32) of Chapter 3.

Figure 4.12 shows one input curve presented in an alternative form ($v(x)$ multiplied by a constant $\frac{2}{k\lambda_0}$) and Figure 4.13 shows another input curve, $g(x)$. For each plot, the discrete simulation points (shown as circles) are very well matched with a solid curve found by poly fitting these values in a least-squares sense.

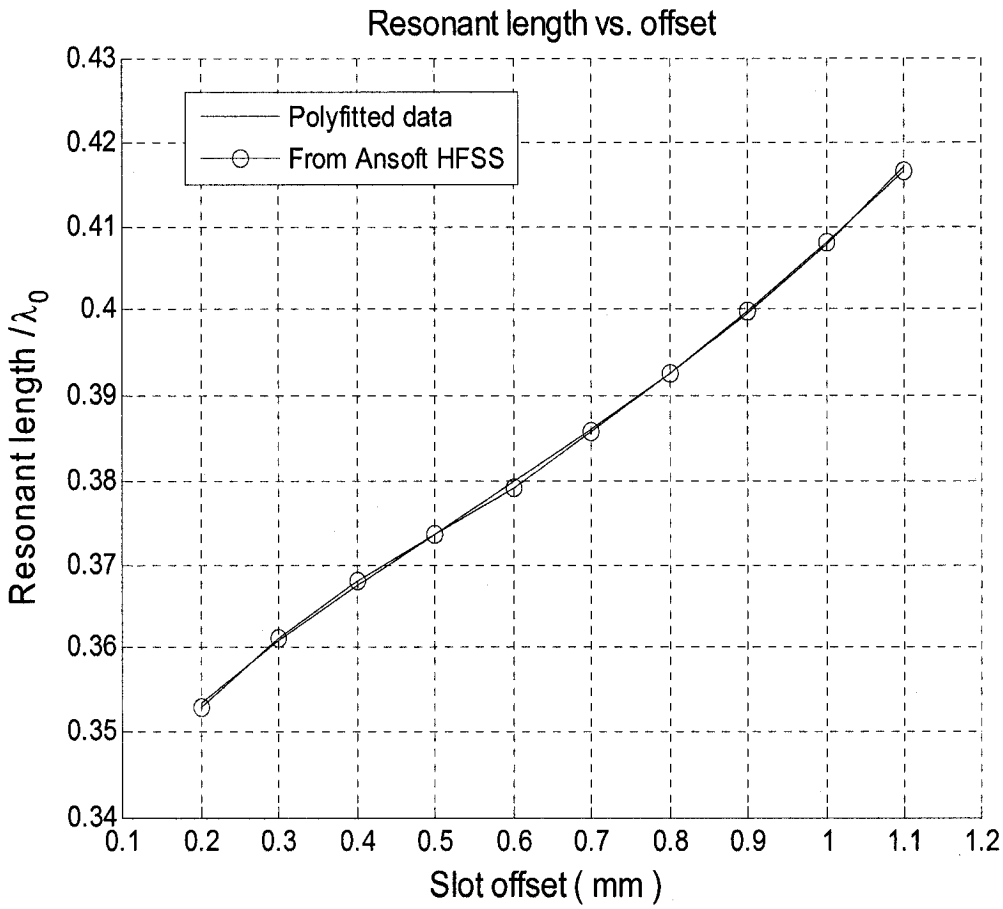

Figure 4.12: Normalized resonant length as a function of offset; polyfitting.

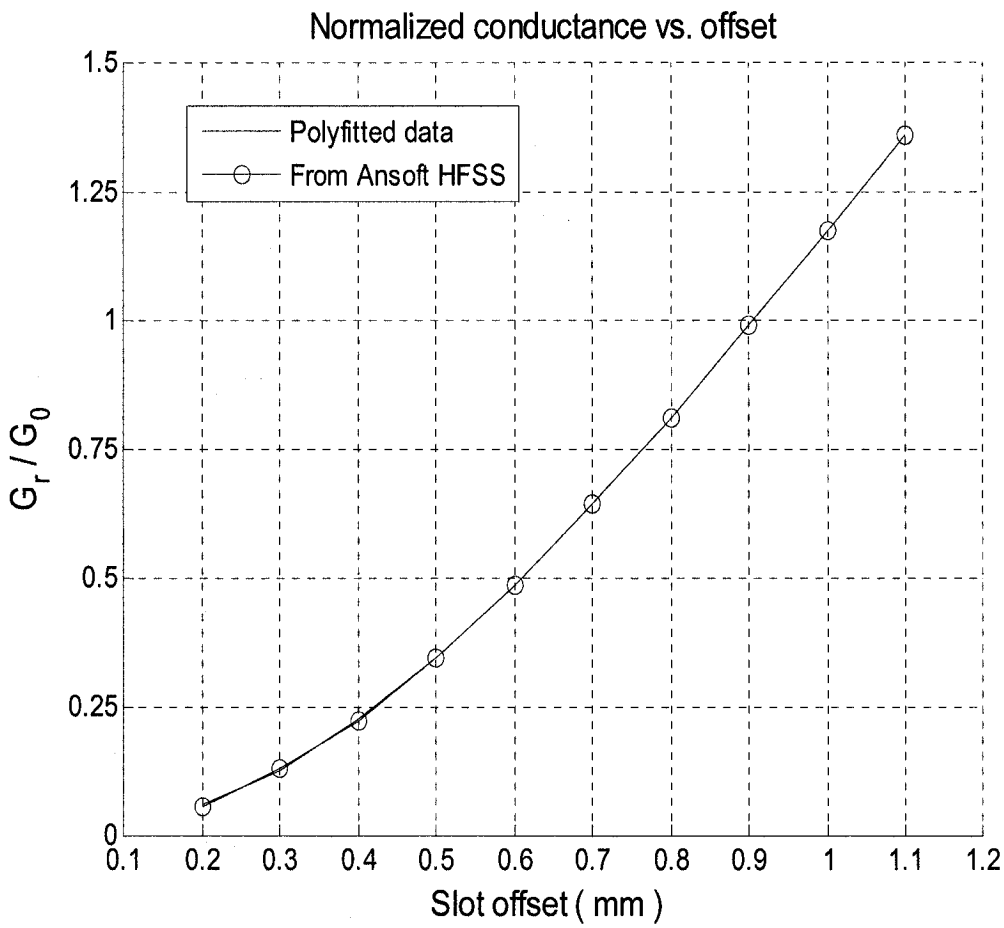

Figure 4.13: Normalized resonant conductance $(g(x))$ as a function of offset; polyfitting.

Figure 4.14 and Figure 4.15 show conductance and susceptance $(h_1(y)$ and $h_2(y))$ both normalized to resonant conductance versus normalized length. A study of $h_1(y)$ and $h_2(y)$ - each at two different offsets show that $h_1(y)$ and $h_2(y)$ are essentially independent of offset.

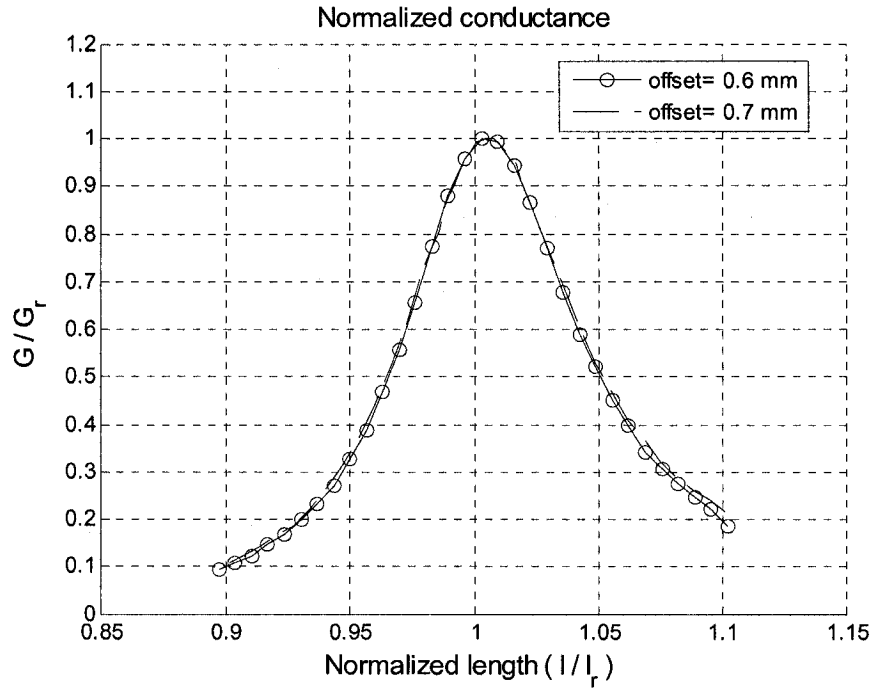

Figure 4.14: Comparison of $h_1(y)$ as a function of y at two different offsets.

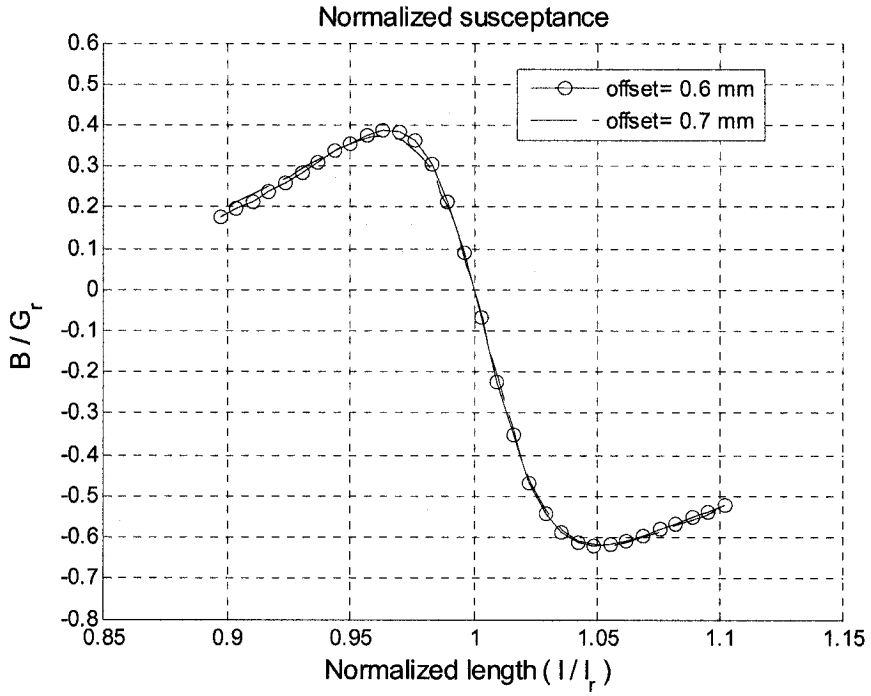

Figure 4.15: Comparison of $h_2(y)$ as a function of y at two different offsets.

The functions $h_1(y)$ and $h_2(y)$ at an average offset of 0.6 mm that have been used in design of the array means those for any value of offset in the range, 0.2 mm to 1.1 mm. Figure 4.16 and Figure 4.17 show these curves. Piecewise polyfitting has been used to match these curves over the range of y since a single expression for entire range causes a much deviated shape from the simulated result points.

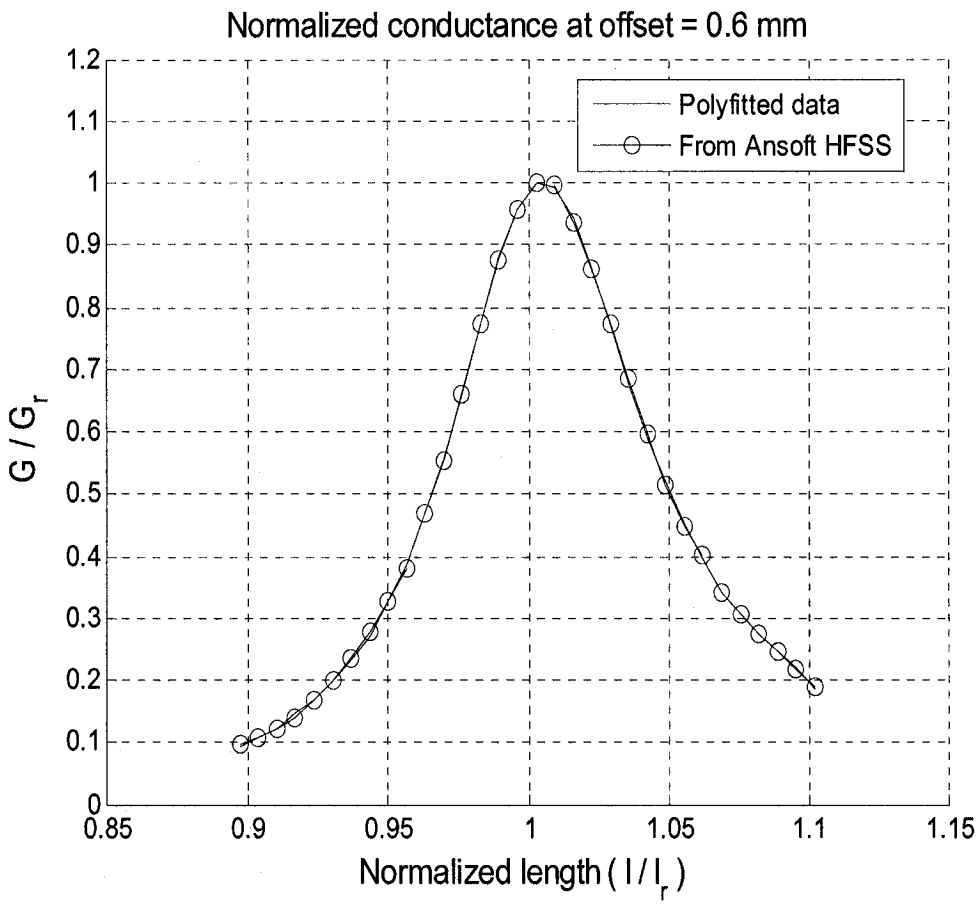

Figure 4.16: $h_1(y)$ at offset = 0.6 mm; polyfitting.

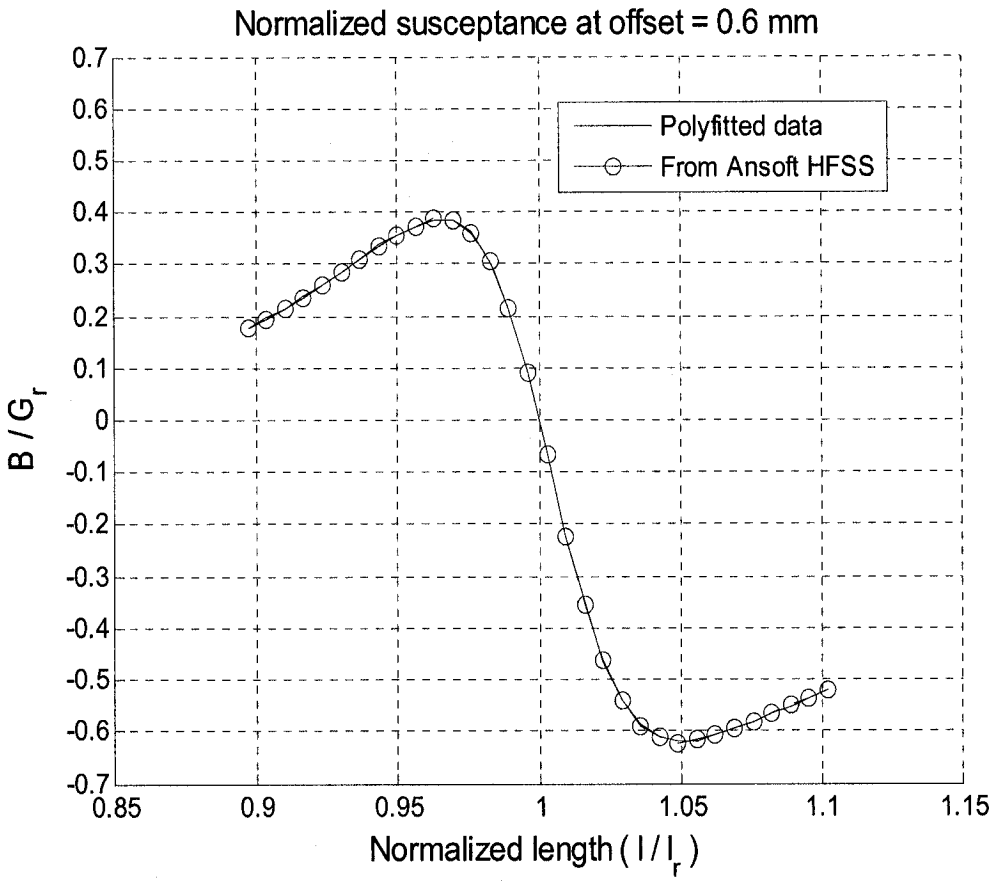

Figure 4.17: $h_2(y)$ at offset = 0.6 mm; polyfitting.

Chapter 5

Numerical results II: Linear arrays of longitudinal slots on SIW

5.1 Introduction

In many applications it is necessary to design antennas with high directivity characteristics to meet the demand of long distance communication. This can only be accomplished by increasing the electrical size of the antenna. The useful way to enlarge the dimensions of the antenna, without necessarily increasing the size of the individual elements, is to form an assembly of radiating elements. This new antenna, formed by multielements, is referred to as an array. In most cases, the elements of an array are identical. The relative physical positioning of the elements and their relative electrical excitations are two parameters that can be used to exercise control over the shape of the radiation pattern of an array.

In the area of microwave antennas, the waveguide resonant slot array antenna, which has advantages of good direction of radiation, low cross-polarization levels and low side-lobe levels, play an important role. By transferring the conventional waveguide resonant slot array antenna to the substrate integrated waveguide (SIW) structure, we can get the advantages of the resonant slot array antenna as well as the advantages of the SIW such as small size, low profile, low cost.

This chapter mainly focuses on the results of arrays of longitudinal slots on SIW. First the definitions of resonant and non-resonant slot arrays is clarified. The connection of slot voltage distribution with design parameters -length and offset of each slot, is

reviewed and the technique to determine the slot voltage distribution is outlined. Then simulated results of patterns and bandwidth for a uniform array of four slots and array with -20 dB SLL of four slots are presented.

A feed system for uniform array of four slots on SIW is designed and optimized. An array with eight elements is designed for uniform distribution and results of simulation is presented.

5.2 Two basic types of slot array

Depending on the spacing between elements and type of termination (either matched or shorted) slot arrays fall into two categories -Resonant Arrays and Non-Resonant Arrays. The fields set up in the waveguide differ due to the different terminations and consequently they require different design procedures.

5.2.1 Resonant Arrays

In a resonant slot antenna array, elements are excited in the standing wave mode and hence the name resonant array. All the elements are half-guide wavelength ($\lambda_g / 2$) apart and are placed alternately on the either side of the guide axis for broadside operation (all slots on the same side of the axis give end-fire beam). Spacing the slots at half-guide wavelength intervals in the waveguide is an electrical spacing of 180° - each slot is exactly out of phase with its neighbors, so their radiation will cancel each other. However, slots on opposite sides of the centerline of the guide will be out of phase (180°), so that alternating the slot displacement around the centerline results in a total phase difference of 360° between slots, putting them back in phase.

A resonant array is terminated by a short circuit placed quarter guide-wavelength apart from the centre of the last slot and thus locates the slots at standing-wave peak.

Figure 5.1 shows a resonant array of longitudinal slots and Figure 5.2 shows its equivalent circuit.

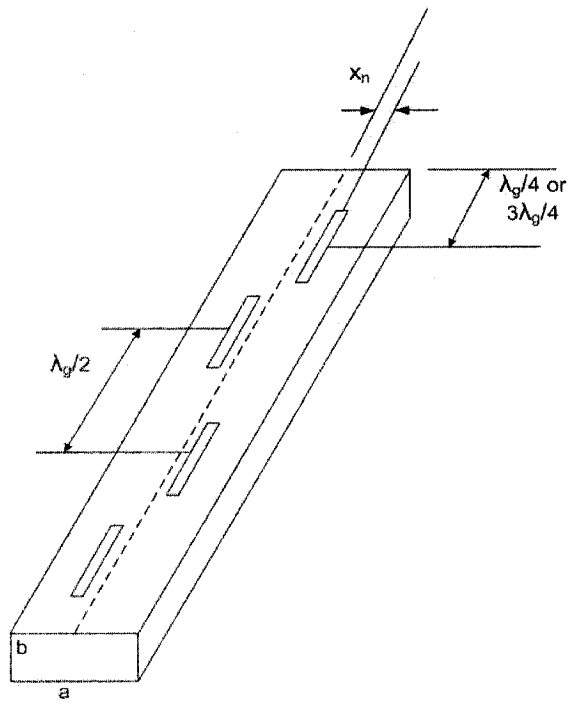

Figure 5.1: A resonant array of longitudinal slots.

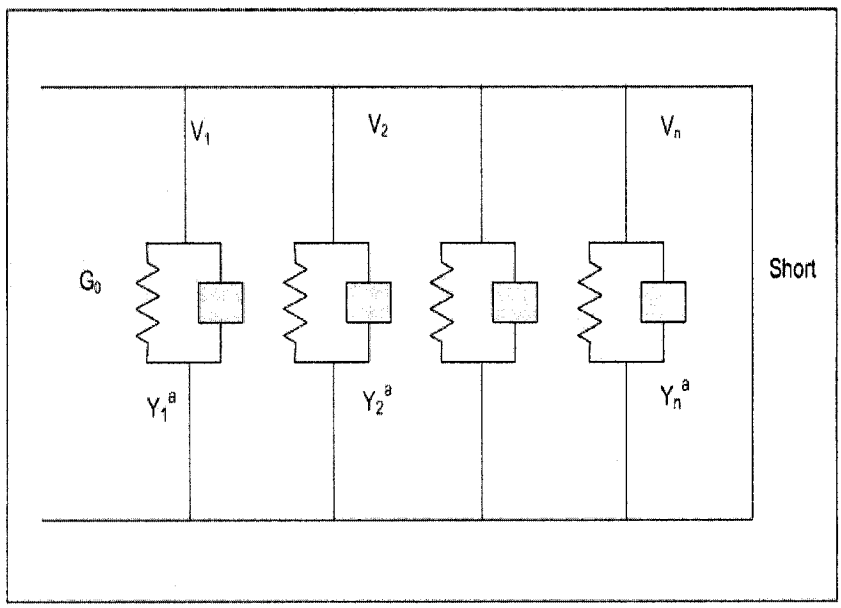

Figure 5.2 : Equivalent circuit of a resonant array of longitudinal slots.

We know that a short-circuited quarter-wavelength stub of transmission line appears as an open-circuit, so that the closed end does not affect the impedance. Sometimes the closed end is spaced at three quarter of guide-wavelength for mechanical reasons; the additional half-wavelength is transparent.

A half-wavelength of transmission line has the useful property of repeating impedance, the input and output impedance are the same. As a result, the impedances, or admittances, of all the slots appear in parallel.

The resonant array yields an accurate normal beam at the design frequency and is well matched at this frequency. The impedance match however deteriorates rapidly with departure from the resonant frequency and the array can be used over a narrow frequency bandwidth.

5.2.2 Non-Resonant Arrays

The non-resonant slot array antenna may consist of a number of elements spaced a little more or little less than $\lambda_g/2$. Consequently slots are not in phase and the beam is not normal to the array axis but is tilted.

Like the resonant array, a non-resonant array also employs resonant slots as basic radiators; the difference lies in the method of terminating the array. The non-resonant array is terminated in a matched load and thus all the slots are excited in the traveling-wave mode.

5.3 Determination of amplitude distribution of array elements

For a broadside array, the maximum radiation of the array is directed normal to the axis of the array. To have the maximum of the array in the broadside direction, it is necessary that all the elements have the same phase excitation [42].

A model of our antenna may be constructed by considering the slots as shunt admittances linked by sections of ideal transmission lines, as shown in Figure 5.2. The aim of the design procedure is to determine the length and offset of each slot in such a way as to achieve the desired voltage distribution on the different slots. The design rests on two equations which are repeated below from Chapter 3.

$$\frac{Y_n^a}{G_0} = K_1 f_n \frac{V_n^s}{V_n} \tag{5.1}$$

$$\frac{Y_n^a}{G_0} = \frac{2f_n^2(x_n, l_n)}{\frac{2f_n^2(x_n, l_n)}{Y(x_n, l_n)/G_0} + MC_n} \tag{5.2}$$

All the terms appeared in these two equations have already been defined in Chapter 3.

It is evident from equation (5.1) that slot voltage of n^{th} slot, V_n^s, is connected to normalized active admittance, $\frac{Y_n^a}{G_0}$ of slot n, mode voltage, V_n of slot n and f_n a constant which depends on the slot length $2l_n$ and offset x_n.

The pattern is independent of the level of the required voltages, V_n^s; The design procedure (Section 3.5) uses the ratios of equation (5.1) for different values of n to remove this uncertainty. For two different slots p and n, equation (5.1) in ratio form can be written as

$$\frac{Y_p^a / G_0}{Y_n^a / G_0} = \frac{f_p}{f_n}\frac{V_p^s}{V_n^s}\frac{V_n}{V_p}. \qquad (5.3)$$

So the slot voltages appear in ratio form in equation (5.3). Now if there are N slots spaced $\lambda_g/2$ apart, the mode voltage V_n has a common value (except for an alternation in sign) for all slots. From equation (5.1), this alternation of sign is compensated by an alternation in the direction of slot offset, which causes $\sin(\frac{\pi x_n}{a})$ in f_n to change sign at successive slots. For a broadside pattern, the slot voltage V_n^s will have same phase for slots. Then equation (5.3) indicates that all the active admittances $\frac{Y_n^a}{G_0}$ should have the same phase. In such circumstances, the usual choice is to make $\frac{Y_n^a}{G_0}$ pure real for all *n*.

Design of resonant arrays requires the ratio of slot voltages to be known. The slot voltage distribution is determined by the pattern specification. Since the phases of excitation of all slots are same for a broadside array, only the amplitudes of excitation are to be determined. For a uniform array, as by definition, all slots will have same excitation-amplitude. But for a broadside array with a low value of symmetric side-lobe level (SLL), the amplitude of excitation will be nonuniform and symmetric with respect to the center of the array. To design a broadside array with a low value side-lobe level (SLL), one of the popular synthesis techniques like Dolph-Chebyshev distribution or Taylor's distribution can be adopted.

For this thesis, a Dolph-Chebyshev distribution [42] has been used to design a broadside array with symmetric -20 dB SLL. Dolph's procedure matches finite terms of Fourier series of array factor with the terms of like degree of a Chebyshev

polynomial. The polynomial chosen should be of order one less than the total number of elements of the array.

5.4 Simulation results using HFSS

A linear broadside array has been designed with four slots for uniform amplitude distribution. The main side lobes for a uniform array should be around 13.46 dB below the peak beam [42]. Also a broadside array has been designed for – 20 dB SLL with four slots. The nonuniform excitation coefficient (slot voltage ratio) has been determined using Dolph-Chebyshev technique.

Figure 5.3 shows a four-slot linear array with element numbering as shown. For symmetrical slot voltage distribution, slots 1 and 4 will have the same length and opposite offsets, as will slots 2 and 3.

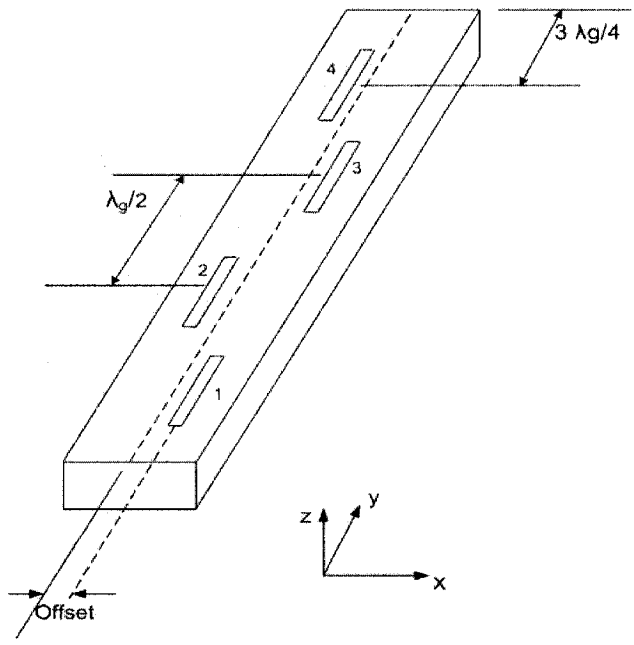

Figure 5.3: Linear array of four longitudinal slots.

Though via holes necessitates a lot of processing time for simulation, all simulations have been performed on SIW (waveguide with via holes).

5.4.1 Linear uniform array of four slots

For a uniform distribution, all slot voltages have same amplitude. The design procedure as discussed in Chapter 3 has been followed including the effect of mutual coupling to determine the lengths and offsets (displacements from center line of waveguide) for all slots. The lengths and offsets thus obtained have been used to simulate the slot waveguide structure by Ansoft HFSS [3]. The section of waveguide with four slots is $3\lambda_g$ long. For orientation of axes as shown in Figure 5.3, the *E*-plane is the yz-plane ($\phi = 90^0$) and the *H*-plane is the xz-plane ($\phi = 0^0$). A positive elevation angle (positive θ) is the angle from $+z$-axis to $+y$-axis, whereas a negative elevation angle (negative θ) is the angle from $+z$-axis to $-y$-axis.
Careful tuning is required to have a perfect pattern as well as good input matching.

The design parameters are,

- ***Lengths of slot 1 and 4 = 3.755 mm***
- ***Displacements of slot 1 and 4 from center line of broadwall of SIW (Offset) = 0.525 mm***
- ***Lengths of slot 2 and 3 = 3.70 mm***
- ***Displacements of slot 2 and 3 from center line of broadwall of SIW (Offset) = 0.525 mm***
- ***Slot width = 0.25 mm***

Figure 5.4 shows the *E*-plane pattern which is of principal interest. The pattern shows symmetrical SLL of -13.5 dB. Figures 5.5 and 5.6 show polar plots of *H*-plane and azimuth patterns. The azimuth pattern shows symmetry about $\phi=90^0$ axis, i.e., the

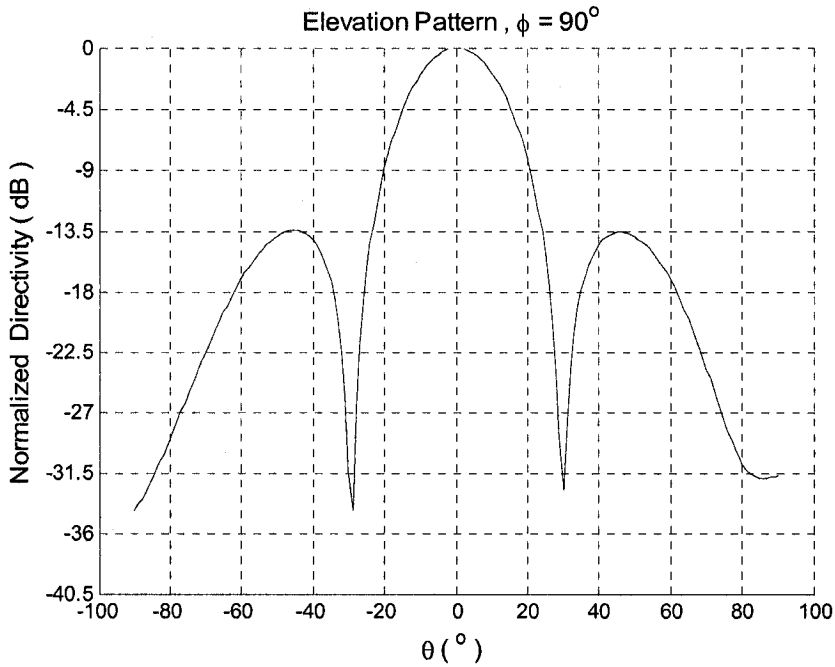

Figure 5.4: *E*-plane pattern, uniform array of four slots.

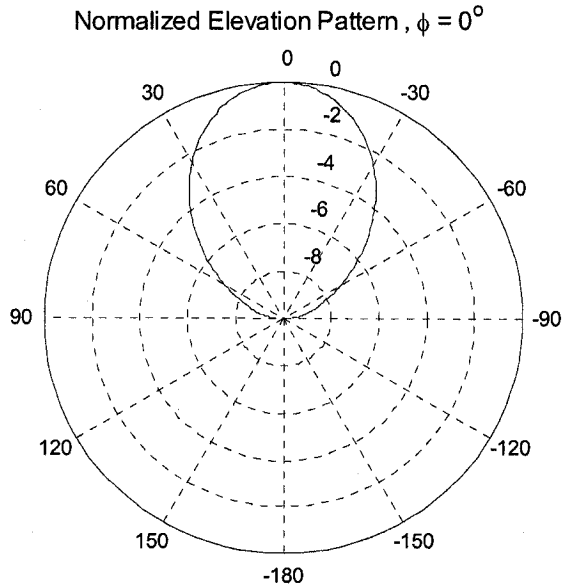

Figure 5.5: *H*-plane pattern (polar diagram), uniform array of four slots.

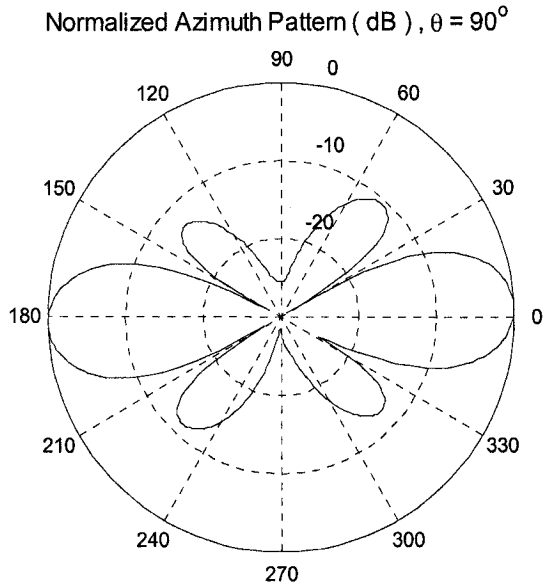

Figure 5.6: Azimuth pattern (polar diagram), uniform array of four slots.

axis of the linear array. Because of presence of broadwall (conducting plane), the gain is very low at this plane.

The frequency bandwidth is fairly limited for a slot array, about 2 to 10 percent [41] depending upon the antenna geometry and the criteria used to define band-limits. The dielectric filling has also the effect of narrowing the slot bandwidth [26]. The return loss of the SIW uniform array antenna was calculated from 28 to 32 GHz, and the result is shown in Figure 5.7. The return loss is less than -10 dB within a wide bandwidth of about 2.7 GHz which implies 9 % bandwidth at center frequency. The resonant frequency is not exactly at 30 GHz due to the approximations taken in the design.

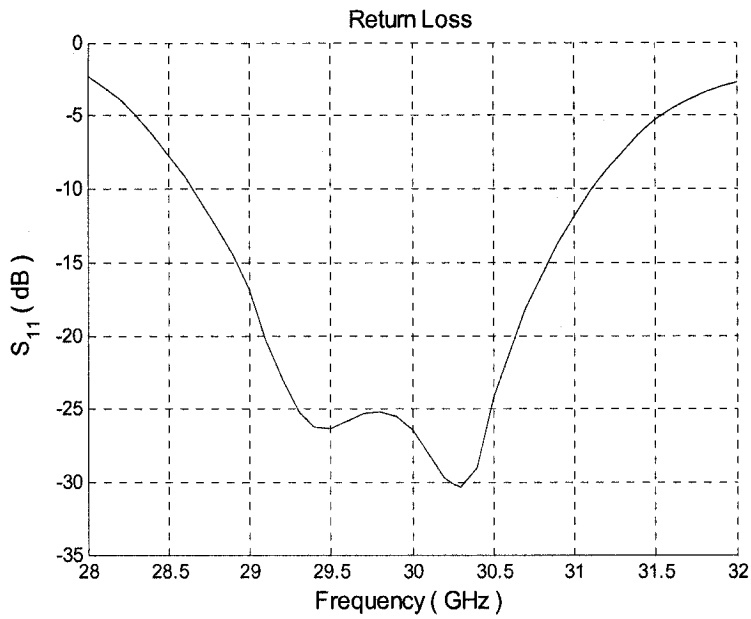

Figure 5.7: Return loss, uniform array of four slots.

5.4.2 Nonuniform linear array of four slots (-20 dB SLL)

For this array, the slot voltage distribution is 1: 1.7357: 1.735 :1 obtained using Dolph-Chebyshev distribution technique as mentioned in Section 5.3. The design procedure of Chapter 3 has been followed including the effect of mutual coupling to determine the lengths and offsets for all slots. Ansoft HFSS [3] has been used to simulate the slot array. The section of waveguide with four slots is $3\lambda_g$ long.

The design parameters are,

- ***Lengths of slot 1 and 4 = 3.68 mm***
- ***Displacements of slot 1 and 4 from center line of broadwall of SIW (Offset) = 0.450 mm***
- ***Lengths of slot 2 and 3 = 3.70 mm***
- ***Displacements of slot 2 and 3 from center line of broadwall of SIW (Offset) = 0.565 mm***
- ***Slot width = 0.25 mm.***

Figure 5.8 shows the *E*-plane pattern which is of principal interest. The pattern shows symmetrical SLL of -20 dB. The *H*-plane pattern and azimuth pattern (not shown) are almost similar to those for uniform array.

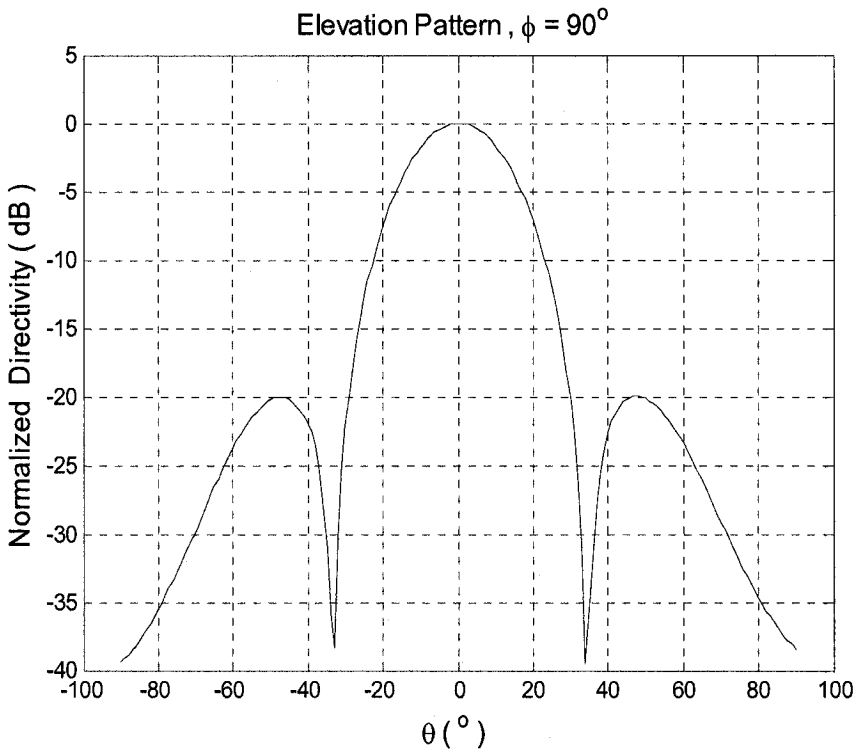

Figure 5.8: *E*-plane pattern, nonuniform array of four slots.

The return loss of the SIW array antenna with tapered symmetrical excitation distribution for -20 dB SLL was calculated from 28 to 32 GHz, and the result is shown in Figure 5.9. The bandwidth for return loss better than -10 dB is about 2.6 GHz which implies 8.67% bandwidth at center frequency. Again the best input matching is found to occur at slightly above 30 GHz.

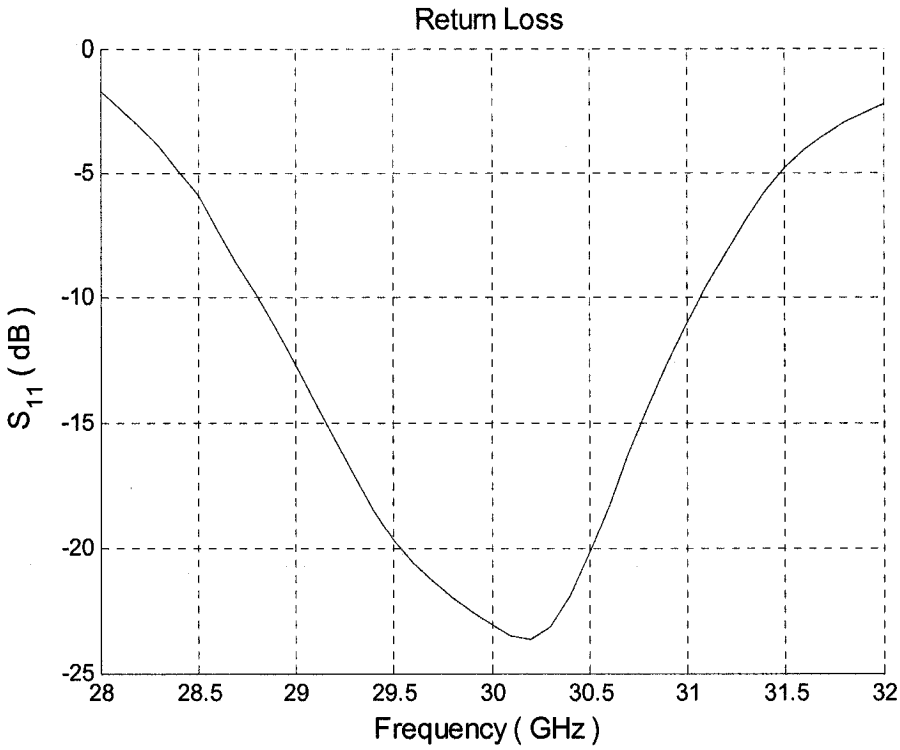

Figure 5.9: Return loss, nonuniform array (-20 dB SLL)

of four slots.

5.4.3 Scope of scanning

Unlike a broadside or end-fire array, for a scanning or phased array the maximum radiation is directed to a particular target direction. It can be achieved by controlling the phase between successive elements. Let the maximum radiation be oriented at an angle θ_0 ($0^0 \leq \theta_0 \leq 180^0$). To accomplish this, the phase excitation between elements must be adjusted so that

$$\delta = -kd\sin\theta_0 \qquad (4.4)$$

Where δ is the progressive phase difference between successive elements, k is the free-space wave number, d is the separation distance between elements; angle θ_0 is being measured from the normal to array-axis. So for a particular angle of main beam,

both d and δ are to be known. For the resonant array discussed so far, if the frequency is changed significantly, the spacing between elements remains no longer at $\lambda_g / 2$ for that frequency. As a result, the slots are not in phase and the main beam is tilted.

Figures 5.10 and 5.11 show the tilting of beam in positive and negative direction respectively through frequency variation. A uniform amplitude distribution is used for the following simulations using Ansoft HFSS [3]. Dimensions used are same as that of Section 5.4.1.

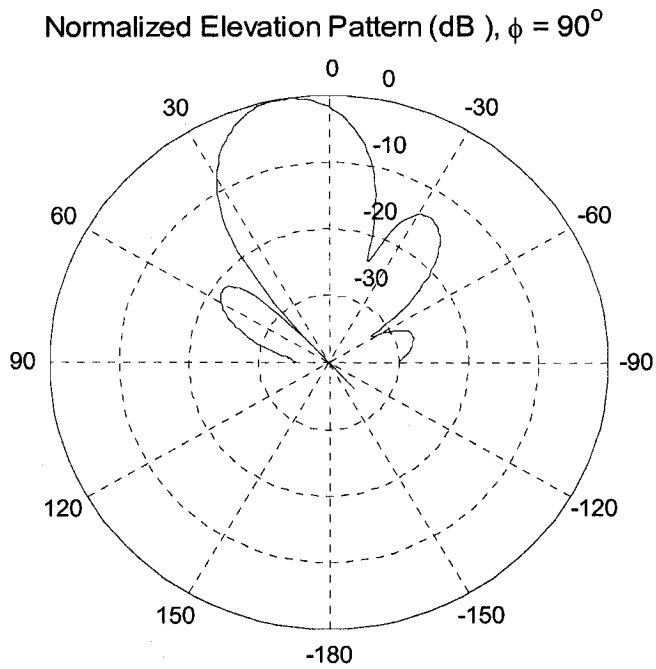

Figure 5.10: *E*-plane pattern (polar diagram), main beam at 10^0, frequency = 33 GHz.

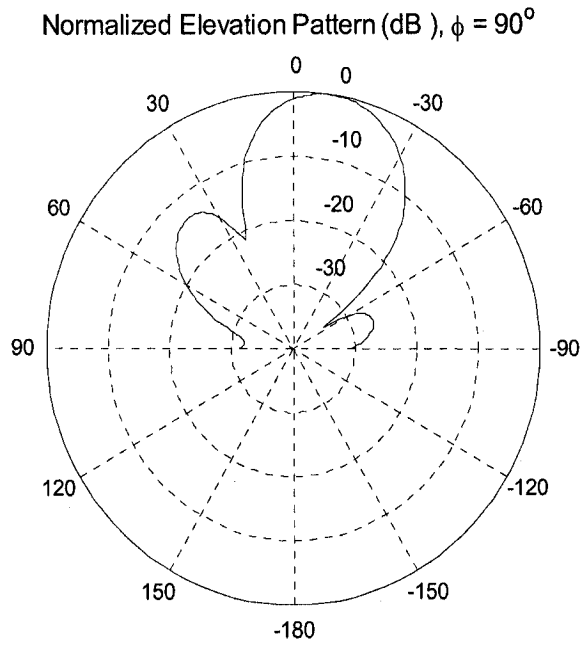

Figure 5.11: *E*-plane pattern (polar diagram), main beam at -10^0, frequency = 27 GHz.

As discussed in Section 5.2.2, scanning for a slot array occurs when the spacing between elements d is not $\lambda_g/2$ and the array is terminated with a matched load for traveling-wave mode excitation. The design of such an array, to obtain the optimum lengths and offsets for a particular target angle, a control over side-lobe level and input matching without generating grating lobes, is in fact a voluminous job and falls under the broader category of traveling wave array design. But the effect of changing d with a matched load termination was observed to produce tilting of the main beam as shown in Figures. 5.12 and 5.13.

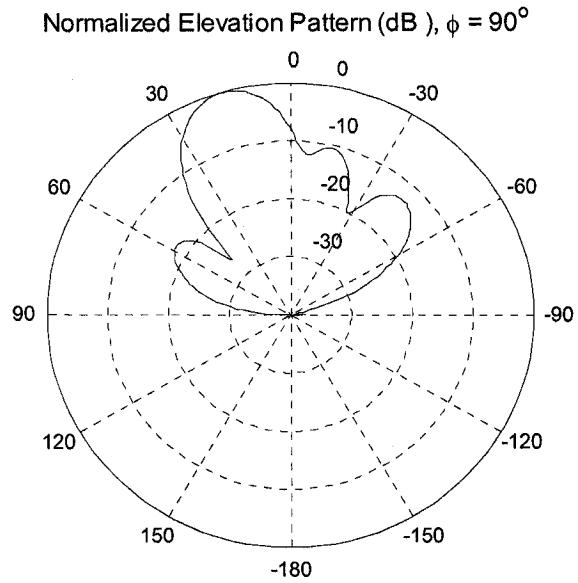

Figure 5.12: *E*-plane pattern (polar diagram), main beam at 15^0,

$$d = 0.778(\lambda_g / 2).$$

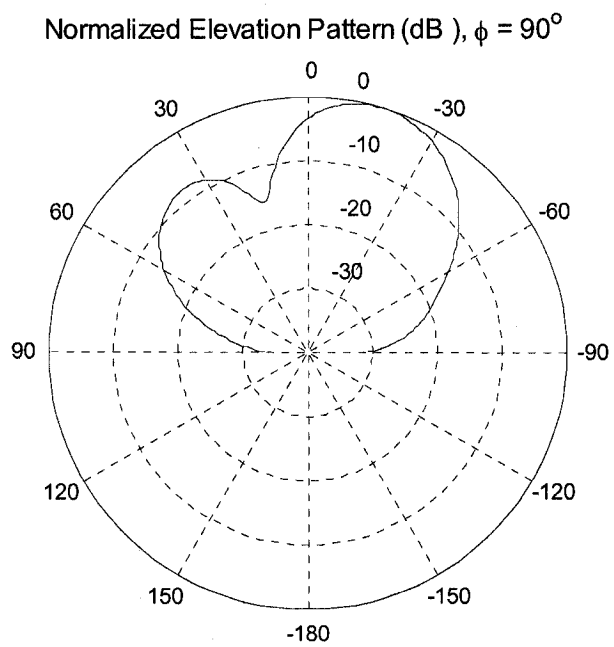

Figure 5.13: *E*-plane pattern (polar diagram), main beam at -15^0,

$$d = 1.335(\lambda_g / 2).$$

5.4.4 Design of transition between waveguide and microstrip line

We have adopted the transition proposed by Deslandes *et al.* [33] in which the microstrip line and rectangular waveguide are fully integrated on the same substrate. The transition structure makes use of a tapered microstrip line to excite the waveguide mode of the SIW. The taper is used to transform the quasi-TEM mode of the microstrip line into the TE_{10} mode in the waveguide. Figure 5.14 shows the diagram of such a transition.

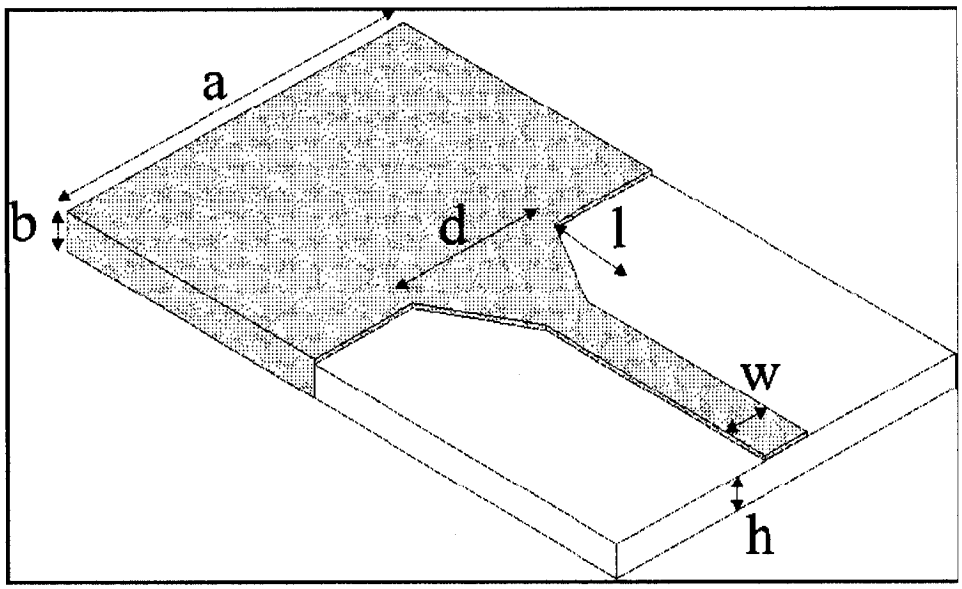

Figure 5.14: Transition of microstrip line to rectangular waveguide on the same substrate [33].

A tapered microstrip line having a characteristic impedance of 75 ohm was used to feed the uniform array of four slots on SIW from one side, the other side being a short circuit. The dimension w which is the width of microstrip line depends on height and dielectric constant of the substrate. Using formula from [43] for microstrip line design, with $b = h = 1.575\ mm$ and $\varepsilon_r = 2.2$, for Rogers /RT Duroid 5880 substrate that we used for SIW, we get $w = 2.506\ mm$.

The dimension l should be near to that of a quarter wavelength transformer. The substrate has a effective dielectric constant [43], $\varepsilon_{eff} = 1.8053$ and thus l should be around 1.8593 mm. Ansoft HFSS [3] has been used to make a careful tuning of w, l and d to optimize return loss while retaining pattern fidelity. The final dimensions of the tapered transition for feeding the uniform array are,

- $w = 2.51\,mm$
- $l = 1.814\,mm$
- $d = 3.02\,mm.$

Other dimensions are same as that of Section 5.4.1.

Figure 5.16 shows the *E*-plane pattern for a four-slot uniform array with feed system as shown in Figure 5.15.

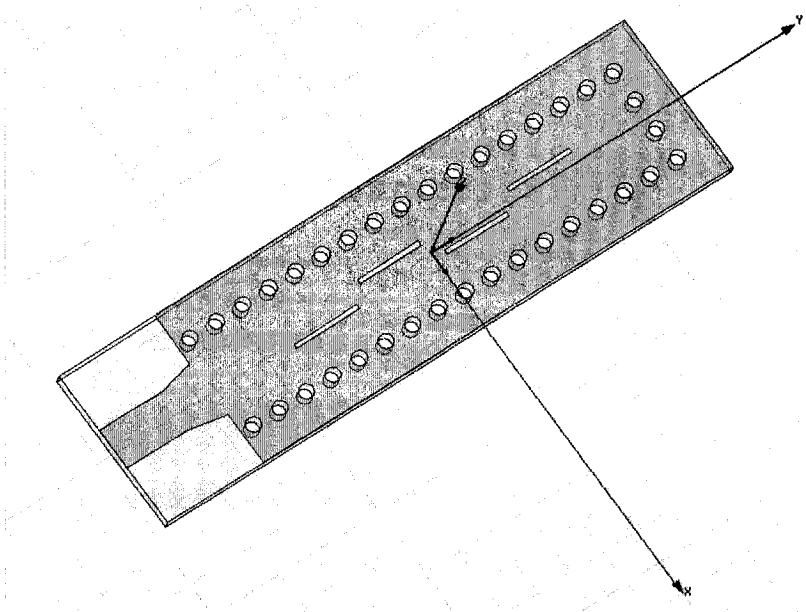

Figure 5.15: Slot array antenna on SIW with tapered microstrip transition.

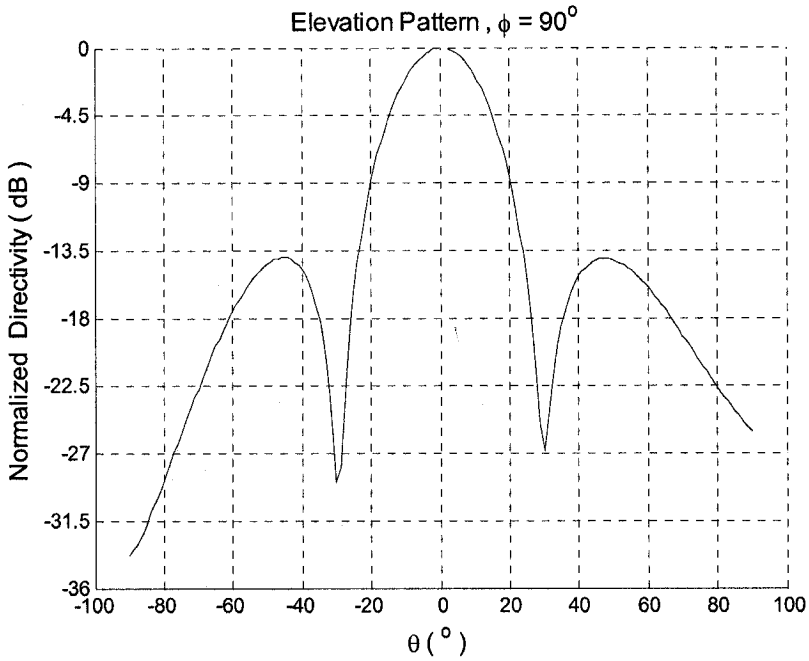

Figure 5.16: *E*-plane pattern of a four-slot uniform array with tapered microstrip feed.

Figure 5.17 shows the return loss of four-slot uniform array on SIW including this transition.

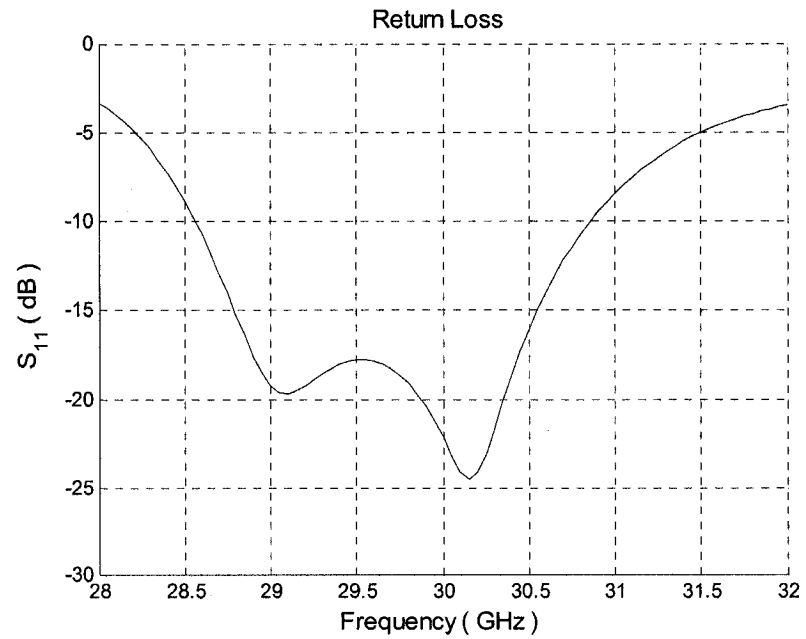

Figure 5.17: Return loss including transition.

A comparison of Figure 5.17 with Figure 5.7 show that, inclusion of transition has slightly degraded the matching and bandwidth is reduced by about 0.11 GHz.

5.4.5 Effect of slot width on the array's bandwidth

The slot is by itself narrow-band with the bandwidth further reduced in the array by the mutual coupling among the slots [38]. The dielectric constant reduces the bandwidth more [26]. For a narrow slot, the width of the slot should be narrow compared to both wavelength and length of the slot. Stegen's measurement data [6] shows that he used $\frac{Slot\ \ length}{Slot\ \ width} > 10$ for an air-filled waveguide at *X*-band. An estimate of resonant length of slot for dielectric–filled waveguide is given [27] as

$$l_r = \frac{\lambda_0}{\sqrt{2(\varepsilon_r + 1)}}. \qquad (5.5)$$

If slot length is given by equation (5.5), then, Gatti *et al.* [26] used $\frac{Slot\ \ length}{Slot\ \ width} \approx 12$ for a dielectric–filled waveguide and Lu and Chu [40] used $\frac{Slot\ \ length}{Slot\ \ width} \approx 13$ for an SIW.

The structure of Figure 5.15 was simulated using HFSS [3] with three different slot widths - 0.25 mm, 0.35 mm, 0.45 mm that correspond $\frac{l_r}{w}$ equals to 15.8, 11.28 and 8.78 respectively. The return loss for three cases is shown in Figure 5.18 for a frequency range from 28 to 32 GHz. It can be observed that gain in bandwidth (for return loss less than -10 dB) with a higher slot width is not significant. The radiation pattern deteriorates in terms of symmetry and magnitude of side lobe level as the width goes up. It is recommended to retain the original value of slot width i.e., 0.25

mm. At a slot width of 0.45 mm or bigger, the narrowness of the slot becomes questionable.

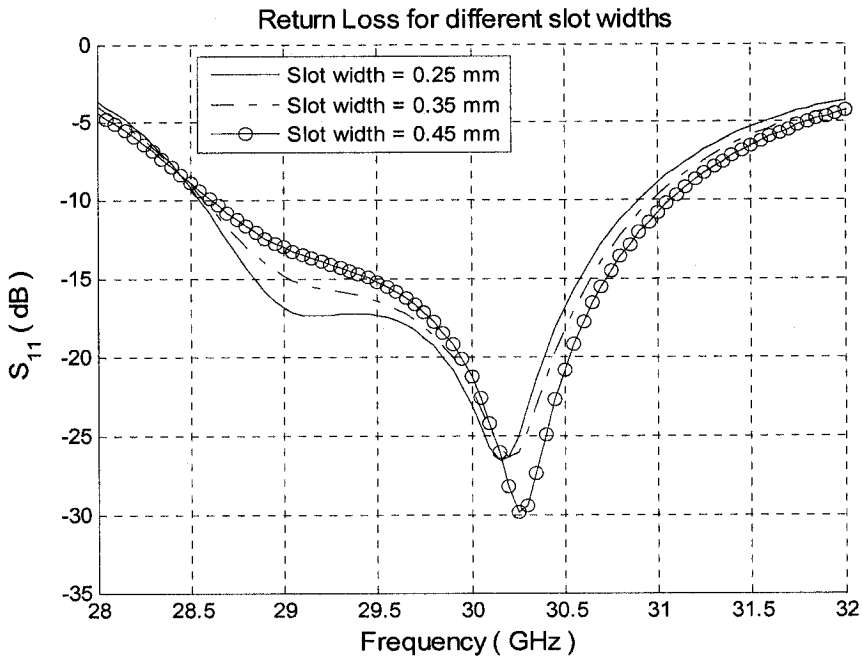

Figure 5.18: Return loss for three different slot widths

5.4.6 Array with eight elements

The design procedure of Chapter 3 has been followed including the effect of mutual coupling to design a broadside uniform array of eight slots on SIW.

Figure 5.19 shows topology of an eight-slot linear array with elements numbering as shown.

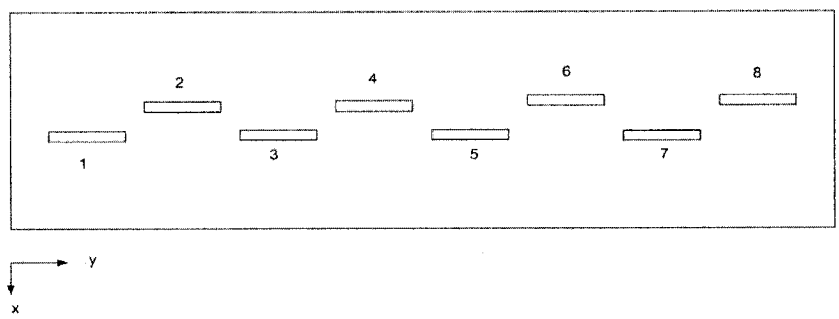

Figure 5.19: Topology of an eight-slot linear array.

For a uniform distribution, all slot voltages have same amplitude. MATLAB has been used in an iterative way to determine the optimum length and offset of all slots that satisfies the design requirements. Ansoft HFSS [3] has been used to simulate the slot-array structure. The section of waveguide with eight slots is $5\lambda_g$ long.

The design parameters are,

- ***Lengths of slot 1, 4, 5 and 8 = 3.65 mm***
- ***Displacements of slot 1, 4, 5 and 8 from center line of broadwall of SIW (Offset) = 0.39 mm***
- ***Lengths of slot 2, 3, 6 and 7 = 3.655 mm***
- ***Displacements of slot 2, 3, 6 and 7 from center line of broadwall of SIW (Offset) = 0.41 mm***
- ***Slot width = 0.25 mm.***

Figure 5.20 shows the *E*-plane pattern for an eight-slot uniform array.

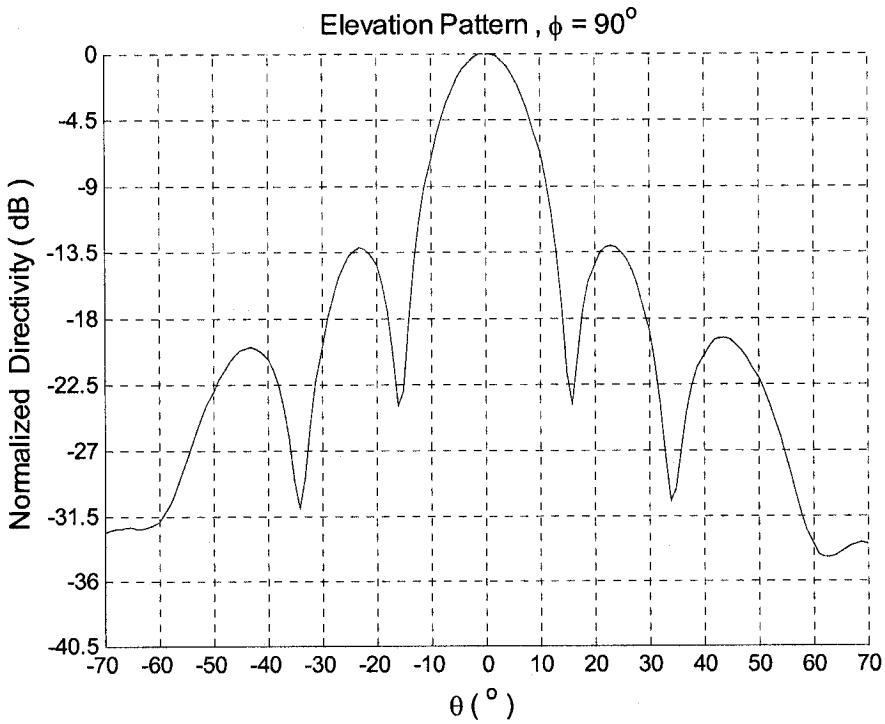

Figure 5.20: *E*-plane pattern, uniform array of eight slots.

With more elements, as expected, the main beam becomes narrower with increased directivity. The return loss of this SIW uniform array antenna was calculated from 28 to 32 GHz, and the result is shown in Figure 5.21. The return loss is less than -10 dB within a wide bandwidth of about 1.8 GHz which implies 6% bandwidth at center frequency.

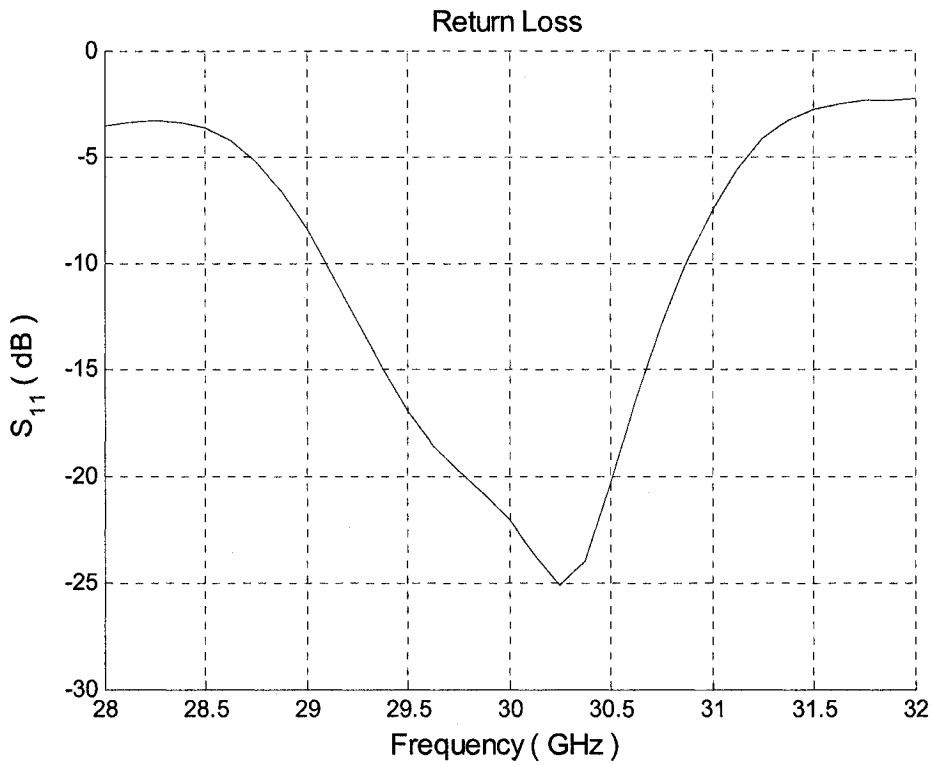

Figure 5.21: Return loss, uniform array of eight slots.

5.4.7 Estimation of half-power beamwidth and directivity

For the three types of linear arrays discussed so far, Table 5.1 shows a comparison of half-power beamwidth predicted by array theory [42] and that obtained from simulation. Theoretical angles at half-power (-3 dB) can be detected from plot of pattern predicted by theory.

Half-power beamwidth	Uniform array with four elements	Uniform array with eight elements	Nonuniform array with four elements
From array theory	24.98^0	12.58^0	28.14^0
From Ansoft HFSS [3] simulation	25.2^0	13.8^0	25.4^0

Table 5.1 : Comparison of half-power beamwidth between theory and simulation

Table 5.2 shows a comparison of directivity predicted by theory [42] and that obtained from simulation results.

Directivity (dB)	Uniform array with four elements	Uniform array with eight elements	Nonuniform array with four elements
From array theory	10.73 dB	13.73 dB	10.69 dB
From Ansoft HFSS [3] simulation	12.14 dB	14.83 dB	13.28 dB

Table 5.2 : Comparison of directivity between theory and simulation

The formulas used for calculation of directivity are approximate. A pattern of half-wavelength dipole is used in place of a slot since a half-wavelength dipole is close to dual of a slot. Moreover, the array theory does not consider the effect of mutual coupling. These are the reasons behind the deviation between theoretical prediction and simulation results.

Chapter 6

Conclusion and future work

6.1 Conclusion

Integration and manufacturability is essential in systems design. Substrate integrated waveguides (SIWs) are now being studied extensively to realize circuits/antennas at millimetre-wave frequencies. SIWs represent alternatives to classical waveguides. Owing to the three dimensional nature of regular rectangular waveguides, they can be difficult to manufacture accurately and integrate with planar circuitry at millimetre-wave frequencies. They are also excessively large at low microwave frequencies. In this thesis, a successful design of a broadside resonant linear array of longitudinal slots on substrate integrated waveguide for uniform and nonuniform excitation has been presented. This thesis has the novelty that it presents the design of nonuniform amplitude distribution for a low side lobe level on substrate integrated waveguide for the first time in addition to uniform amplitude distribution case.

For utilizing the design procedure for a dielectric-filled slot array, the SIW has been converted to an equivalent rectangular waveguide using empirical equations and simulation software, Ansoft HFSS [3]. The results of generated S-parameters - insertion loss per unit wavelength, phase error of transmission coefficient per unit wavelength and return loss, justify this conversion and equivalency and establishes that SIW possesses identical propagation constant and characteristic impedance as those of the derived equivalent rectangular waveguide.

In this thesis, an effective method to generate accurate results of self-admittance data using a shunt equivalent circuit for a slot with the aid of HFSS [3] is proposed and used. The method shows that the design of a slot-array rather becomes simplified as the complexity of computing data for the self-admittance is relaxed. Computational efficiency is achieved using Stegen's factorization for the equivalent admittance which is shown to be in good agreement with published results for a slot on an X-band waveguide at 9.375 GHz. However, the main disadvantage of this method of accumulation of self-admittance data is the requirement of huge processing time even though the processor-speed and memory of computers are good.

The results from HFSS [3] for uniform and nonuniform arrays show good symmetry in the *E*-plane pattern and achieving the desired side lobe level. Return loss results for four-slot uniform and nonuniform arrays show a bandwidth around 9% (for RL less than -10 dB). For an eight-slot uniform array the bandwidth is 6% (for RL less than -10 dB). The corresponding radiation pattern has a narrower beamwidth and higher directivity.

In addition, we investigated and showed the feasibility of a SIW array to generate scanned beam for a variation of frequency. Also at center frequency, variation of spacing between elements with a terminated matched load produced scanning as a traveling-wave array.

A planar platform integrating microstrip line and SIW has been presented, which involves a transition between the two dissimilar structures. Results from simulation show that the bandwidth slightly deteriorates due the mismatch introduced by the transition section but the pattern still shows good symmetry.

An estimation of half-power beamwidth and directivity for the three types of array - uniform array with four elements, nonuniform array with four elements and uniform

array with eight elements show a reasonable match of half-power beamwidth and directivity predicted by array theory and that obtained from simulation.

6.2 Future work

There is adequate scope for future work on substrate integrated waveguide-based antennas. The planar (two dimensional) slot-array antenna on substrate integrated waveguide, has recently been studied but only for uniform aperture distribution. So a planar array with reduced side-lobe-level can be studied for two dimensional control of its pattern. Also there is no work so far on this type of antenna for a narrow–beam generation. And beam steering for this type of antenna with traveling-wave excitation is a potential future research area. Other type of feed systems (like coplanar waveguide) can also be studied.

References

[1] Elliott R., "An improved design procedure for small arrays of shunt slots," IEEE Transactions on Antennas and Propagation, vol. 31, no.1, 1983, pp: 48– 53.

[2] Elliott R., O'Loughlin W., "The design of slot arrays including internal mutual coupling," IEEE Transactions on Antennas and Propagation, vol. 34, no. 9, 1986, pp :1149 -1154.

[3] Ansoft HFSS, Version 9, Ansoft Corporation, Pittsburg, PA, 2004.

[4] Sadiku M.N.O., "Numerical techniques in electromagnetics," chapter 6, Boca Raton, Fla.: CRC Press, 1992.

[5] Stevenson A. F., "Theory of slots in rectangular waveguides," Journal of Applied Physics, vol. 19, 1948, pp. 24-38.

[6] Elliott R. S., "Antenna Theory and design," chapter 8, John Wiley & Sons, N.J., 2003.

[7] Oliner A. A., "The impedance properties of narrow radiating slots in the broad face of rectangular waveguide, Part I-Theory" IRE Transactions on Antennas Propagation, vol. AP-5, 1957, pp. 4-20.

[8] Khac T. B. and Carson C.T., "Impedance properties of a longitudinal slot antenna in the broad face of a rectangular waveguide," IEEE Transactions on Antennas and Propagation, vol. 21, no. 5, 1973, pp :708 - 710.

[9] Chao Liu, Benqing Gao and Zhenghui Xue, "Analysis of longitudinal slots-array in rectangular wave-guide with FDTD," Radar, 2001 CIE International Conference on, Proceedings 2001, pp :1103 - 1107.

[10] Brown K.W, "Design of waveguide slotted arrays using commercially available finite element analysis software," Antennas and Propagation Society International Symposium, 1996. AP-S. Digest, vol. 2, 1996, pp :1000 – 1003.

[11] Elliott R., Kurtz L., "The design of small slot arrays," IEEE Transactions on Antennas and Propagation, vol. 26, no.2, 1978, pp : 214 – 219.

[12] Sangster A.J., McCormick A.H.I., "Theoretical design/synthesis of slotted waveguide arrays," Microwaves, Antennas and Propagation, IEE Proceedings H, vol. 136, no.1, 1989, pp :39 –46.

[13] Yee H.Y., "The design of large waveguide arrays of shunt slots," IEEE Transactions on Antennas and Propagation, vol. 40, no. 7, 1992, pp : 775 –781.

[14] Bastani A., Rashed-Mohassel J., "Analysis of planar slotted-waveguide array antennas with longitudinal slots using the Method of Moments," Antennas and Propagation Society Symposium, IEEE, vol. 1, 2004, pp : 129 - 132.

[15] Giulio Antonini, Antonio Ciccomancini Scogna, Antonio Orlandi, "Equivalent Network Synthesis for Via Holes Discontinuities," IEEE Transactions on Advanced Packaging, vol. 25, no. 4, 2002, pp : 528 – 536.

[16] Dongsoo Koh, Hong-Bae Lee, and Itoh T., "A hybrid full-wave analysis of via-hole grounds using finite-difference and finite-element time-domain methods," IEEE Transactions on Microwave Theory and Techniques, vol. 45, no. 12, 1997, pp : 2217 – 2223.

[17] Laso M.A.G., Lopetegi T., Bacaicoa M., Hernandez J., Garde M.J., and Sorolla M., "Arrangements of via-holes in microstrip lines as metallodielectric periodic structures," Microwave Conference, Asia-Pacific, 2000, pp :1257 - 1260.

[18] Uchimura H., Takenoshita T., and Fujii M., "Development of a laminated waveguide," IEEE Transactions on Microwave Theory and Techniques, vol. 46, no. 12, Part 2, 1998, pp: 2438 – 2443.

[19] Zeid A., Baudrand H., "Electromagnetic scattering by metallic holes and its applications in microwave circuit design," IEEE Transactions on Microwave Theory and Techniques, vol. 50, no. 4, 2002, pp :1198 - 1206.

[20] Cassivi Y., Perregrini L., Arcioni P., Bressan M., Wu K., and Conciauro G. "Dispersion Characteristics of Substrate Integrated Rectangular Waveguide," IEEE Microwave and Wireless Components Letters, vol.12, no. 9, 2002 pp : 333 – 335.

[21] Deslandes D. and Wu K., "Design considerations and performance analysis of substrate integrated waveguide components," 32nd European Microwave Conference, Milan, Italy, 2002, pp. : 881–884.

[22] Yu Lin Zhang, Wei Hong, Feng Xu, Ke Wu and Tie Jun Cui, "Analysis of Guided-Wave Problems in Substrate Integrated Waveguides – Numerical Simulations and Experimental Results," Microwave Symposium Digest, 2003 IEEE MTT-S International, vol. 3, 2003, pp : 2049– 2052.

[23] Deslandes, D. and Wu, K., "Single-Substrate Integration Technique of Planar Circuits and Waveguide Filters," IEEE Transactions on Microwave Theory and Techniques, vol. 51, no. 2, Part 1, 2003, pp. : 593-596.

[24] Cassivi Y., Wu K., "Low cost microwave oscillator using substrate integrated waveguide cavity," Microwave and Wireless Components Letters, IEEE, vol. 13, no. 2, 2003, pp : 48 - 50.

[25] Wenquan Che, Yung E.K.-N., and Ke Wu, "Millimeter-wave ferrite phase shifter in substrate integrated waveguide (SIW)," Antennas and Propagation Society International Symposium, IEEE, vol. 4, 2003, pp : 887 - 890.

[26] Gatti R.V., Sorrentino R., and Dionigi M., "Equivalent circuit of radiating longitudinal slots in dielectric filled rectangular waveguides obtained with FDTD method," Microwave Symposium Digest, IEEE MTT-S International, vol. 2, 2002, pp : 871 - 874.

[27] Farrall A.J., Young P.R., "Integrated waveguide slot antennas," Electronics Letters, vol. 40, no. 16, 2004, pp : 974 – 975.

[28] Stephens D., Young P.R., Robertson I.D., "W-band substrate integrated waveguide slot antenna," Electronics Letters, vol. 41, no. 4, 2005, pp : 165 – 167.

[29] Yan L.,Hong W., Hua G., Chen J., Wu K., and Cui T., "Simulation and Experiment on SIW Slot Array Antennas," IEEE Microwave and Wireless Components Letters, vol. 14, no. 9, 2004, pp : 446-448.

[30] Das B., Prasad K., and Rao K., "Excitation of waveguide by stripline and microstrip-line-fed slots," IEEE Transaction on Microwave Theory Techniques, vol. 34, 1986, pp. : 321–327.

[31] Grabherr W., Huder B., and Menzel W., "Microstrip to waveguide transition compatible with MM-wave integrated circuits," IEEE Transaction on Microwave Theory Techniques., vol. 42, 1994, pp. : 1842–1843.

[32] Ho T. and Shih Y., "Spectral-domain analysis of E-plane waveguide to microstrip transitions," IEEE Transaction on Microwave Theory Techniques., vol. 37, 1989, pp. : 388–392.

[33] Deslandes D. and Wu K., " Integrated Microstrip and Rectangular Waveguide in Planar Form," IEEE Microwave and Wireless Components Letters, vol. 11, no. 2, 2001, pp : 68-70.

[34] Deslandes D. and Wu K., "Integrated transition of coplanar to rectangular Waveguides," Microwave Symposium Digest, 2001 IEEE MTT-S International, vol. 2, 2001, pp : 619 - 622.

[35] Elliott R. S., "Antenna theory and design," chapter 3, John Wiley & Sons, N.J., 2003.

[36] Elliott R. S., "An introduction to guided waves and microwave circuits," chapter 6, Englewood Cliffs, N.J.: Prentice Hall , 1993.

[37] Lo Y., and Lee S., "Antenna Handbook," chapter 12, Van Nostrand Reinhold, New York, 1993,.

[38] Josefsson L., "Analysis of longitudinal slots in rectangular waveguides," IEEE Transactions on Antennas and Propagation, vol. 35, no.12, 1987, pp :1351 – 1357.

[39] Theron I., Cloete J., "On slotted waveguide antenna design at Ka-band," Communications and Signal Processing, 1998. COMSIG '98., Proceedings of the 1998 South African Symposium on, 1998, pp : 425 – 426.

[40] Lu H., Chu T., "Equivalent circuit of radiating longitudinal slots in substrate integrated waveguide," Antennas and Propagation Society International Symposium, 2004. IEEE, vol. 3, 2004, pp :2341 - 2344.

[41] Hung Yee and Richardson, P., "Slotted waveguide antenna arrays," IEEE Antennas and Propagation Society Newsletter, vol. 24, no. 6, 1982, pp : 4 - 8.

[42] Balanis C., "Antenna theory: analysis and design," chapter 6, John Wiley & Sons, New York, 1997.

[43] Pozar D., "Microwave engineering," chapter 3, John Wiley & Sons, New York, 1998.